1.0 Introduction

Microbial strains that are typically found in wastewater include coliform bacteria, *Vibrio*, bacilli and cocci, and are not salt-tolerant (Tchobanoglous, Burton, & Stensel, 2004a). Bacterial survival is for example known to be dramatically reduced in seawater. This could cause problems in the biological treatment of high-salinity wastewaters in activated sludge processes, because sludge production and carbon removal is dependent on microbial activity. High-salinity wastewaters may be produced from specialist industries and from households in which saltwater is used in washroom flushing. The usage of halophiles in biological treatment, which are specialised bacteria that thrive in saline environments, could increase the range of wastewaters that could be treated without having to first reduce the salt content. This would save time and energy. The International Water Association (IWA) Task Group has proposed a number of ASM models (Henze, Gujer, Mino, & van Loosdrecht, 2000) over the past few decades that have become extensively used in modelling the biological kinetics of activated sludge processes. These models have been built on standard Michaelis-Menten bacterial growth models. These models do not describe well the effect of environmental parameters on the growth of halophilic bacteria based on the characterisation data that is available (Tsai et al., 1995). In addition, these ASM models do not explicitly account for hydrodynamic effects which could affect the kinetics of biological treatment processes. Reactors are assumed to be completely-mixed; transient effects and non-steady flows are ignored. Alternative bacterial growth models that are applicable to halophiles need to therefore be sought. These models then need to be integrated together with a hydrodynamic model that describes how the kinetics of the reactions can affect the flow regimes and vice versa. This project seeks to develop a conceptual protocol which can be used to do this, and to implement this protocol in a simple set-up as a preliminary test. A number of candidate models that can be used to describe the growth kinetics of a chosen halophile as a function of temperature, environment salt concentration and pH is first identified. Appropriate models will then be selected and used to calculate a growth rate constant. This rate constant and a representative reaction equation to model bacterial growth will then serve as input to a CFD package to be used to model the flows and reactions in the test domain. In this manner both biological kinetics and hydrodynamic

effects are accounted for. The applicability of pre-existing kinetics-only approaches will then be interpreted in light of the simulation results.

2.0 Literature review

2.1 Biological kinetics

Developing and using predictive models of microbial behaviour is arguably a more efficient way of acquiring the information needed in specifying the design features and operating conditions of the wastewater treatment facilities. Building a model enables microbial growth characteristics to be interpolated from known responses and circumvents having to run scaled-down, dimensionally similar experiments to verify that the intended wastewater processing scheme works. The complexity of real biological systems necessitates making certain simplifying assumptions to reduce that complexity without sacrificing essential details. This inevitably introduces errors in the modelling process, a number of which Baranyi and Roberts (1995) have identified:

1. Completeness error – the model omits certain factors which have a causal relationship to the phenomena being modelled
2. Homogeneity error – the model treats all variables as spatially independent
3. Model function error – the mathematical relationships used in the model do not reflect actual processes

A “good” model can thus be considered as one which balances the need for accuracy on one hand, and computational effort and the need for reference data on the other. As the growth data of individual cells are dependent on cell type-specific characteristics such as geometry and on environmental conditions, it would be more instructive to build a model of population behaviour instead (Williams, 1967). It is this population behaviour which exhibits certain characteristics that are shared across diverse cell populations, eukaryotic and prokaryotic (Williams, 1967). These include (Whiting & Cygnarowicz-Provost, 1992) a “lag phase” during which cells grow but no cell division happens, a “log phase” during which the cell population grows at an exponential rate, and a “stationary phase” in which cells remain at a minimum size

and no cell division occurs at which point the growth curve asymptotes to the horizontal (Zwietering, Jongenburger, Rombouts, & VAN 'T Riet, 1990). Several models have been shortlisted as possible candidates to be used in the kinetic modelling of halophile population growth and are presented below with a short description each. Despite the fact that most models were originally designed for use in food microbiology, the fact that populations of diverse cell species in diverse environments seem to share the same response characteristics suggests the (judicial) use of these models in predicting microbial growth responses in activated sludge.

2.1.1 The model of Whiting and Cygnarowicz-Provost (1992)

Whiting and Provost (1992) conjectured that the transition from a non-dividing bacterial cell to a dividing cell is first order, with a rate constant of k_1:

$$N_{\log} = N_{\lag}\, e^{-k_1 t} \tag{5a}$$

The active cells undergo binary division to result in a geometric increase in population size:

$$N_t = N_{\log}\, 2^{t/G} \tag{5b}$$

The parameter N_t is the population size at time ***t*** during the log phase. The parameter ***G*** is the generation time, which is defined as the duration needed for the population to double in size; this value is not constant throughout the log phase[1]:

$$G = k_2 + k_3 \int_0^t N_t\, dt \tag{5c}$$

The parameter k_2 is the primary generation time and k_3 is a constant. Equation (5c) implies that the generation time will increase as the population size increases in time, such that the growth rate reduces. The transition from the phase of active cell division to cell death and dormancy is also assumed to be first-order, with a rate constant k_4 (the decline parameter):

[1] In the original paper (Whiting & Cygnarowicz-Provost, 1992) a discrete sum was used over hourly intervals; this author modified this equation to use an integral instead for the sake of generalisation.

$$N_{\text{stationary}} = N_{\text{t}}\, e^{-k_4 t} \tag{5d}$$

The authors justify their assumption of first-order transitions by arguing that the physiological processes involved in those transitions contain a single rate-controlling step (Whiting & Cygnarowicz-Provost, 1992). This author would suggest that this is a very restrictive assumption, but would agree with them that sufficient data is typically not available to allow a more elaborate function representing high-order kinetics to be fitted. This is especially so in the context of halophilic bacteria, many of which have yet to be completely characterised.

2.1.2 The model of Grau, Dohányos and Chudoba (1975)

In their paper (Grau, Dohányos, & Chudoba, 1975) the authors describe a their model as a "special case of the broader Monod equation", and developed it specifically for modelling the behaviour of bacteria which break down substrates in activated sludge processes. In the case of the bacteria breaking down a single substrate, of concentration ***S***:

$$-\frac{dS}{dt} = \frac{\mu_{\max} M}{Y} \frac{S}{S + k_s} \tag{6a}$$

The parameters $\mu_{\max}$ denotes the maximum microbial growth rate, ***M*** the biomass concentration, ***Y*** the biomass yield and k_s is the Monod constant. If the ratio of the initial substrate concentration to the initial biomass yield is less than 2, the solution to (6a) is:

$$k_s \ln \frac{S_0}{S} + S_0 - S = \frac{\mu_{\max} M}{Y} t \tag{6b}$$

In the case of the bacteria breaking down multiple substrates, the authors propose that:

$$V = \mathrm{F}\left(\frac{n}{N}\right) \tag{6c}$$

The relative rate of substrate removal is some function ***F*** of the ratio of the number of substrates remaining ***n*** to the number of substrates initially present ***N***. The kinetic model becomes:

$$-\frac{dS}{dt} = k_{n,s} M \left(\frac{S}{S_0}\right)^n \tag{6d}$$

The parameter $k_{n,s}$ is the substrate rate constant for ***n***-order kinetics. The authors provide solutions for the cases $n = 1, 2$:

$$\frac{S}{S_0} = \exp\left(-\frac{k_{1,s} M_0 t}{S_0}\right), \quad n = 1 \tag{6e}$$

$$\frac{S}{S_0} = \left(1 + \frac{k_{2,s} X_0 t}{S_0}\right)^{-1}, \quad n = 2 \tag{6f}$$

2.1.3 The model of Monod

Panikov (2002) provides a concise overview of the model of Monod. If the growth yield factor ***Y*** is defined in terms of the biomass ***m*** and the amount of substrate ***s***:

$$Y = \frac{m - m_0}{s_0 - s} \tag{7a}$$

The subscripts denote the respective quantities at the start. The Monod model states that:

$$\frac{dm}{dt} = \mu m = \mu_{\max} \frac{s}{s + K_s} m \tag{7b}$$

$$\frac{ds}{dt} = -\frac{1}{Y} \frac{dm}{dt} \tag{7c}$$

Equation (7c) has the solution:

$$\mu_{\max} t = \left(1 + \frac{Y K_s}{m_{\max}}\right) \ln \frac{m}{m_0} - \frac{Y K_s}{m_{\max}} \ln\left(\frac{m_{\max}}{m_0} - \frac{m}{m_0}\right) + \frac{Y K_s}{m_{\max}} \ln\left(\frac{m_{\max}}{m_0} - 1\right) \tag{7d}$$

Modifications to the model of Monod are not difficult to apply (Panikov, 2002); the Monod-Ierusalimsky equation provides an additional factor to account for non-competitive inhibition (7e) and substrate inhibition can be accounted for as well (7f):

$$\mu = \mu_{\max} \frac{s}{s + K_s} \frac{K_p}{K_p + p} \tag{7e}$$

$$\mu = \mu_{\max} \frac{s}{s + K_s + \frac{s^2}{K_{ss}}} \tag{7f}$$

2.1.4 Bělehrádek models

Ratkowsky *et al.* in 1982 modelled the temperature-dependence of the microbial growth response with the relation (Ratkowsky, Olley, McMeekin, & Ball, 1982):

$$\sqrt{k} = b(T - T_{\min}) \tag{10a}$$

The parameter ***k*** is the microbial growth rate, ***T*** is the temperature and $T_{\min}$ is the minimum temperature at which growth is possible. The parameter ***b*** is the model parameter. This is a special case of the Bělehrádek equation with $n = 2$ (Ross & McMeekin, 1994):

$$b^n = \frac{k}{(T - T_{\min})^n} \tag{10b}$$

An improvement was suggested (Ratkowsky, Lowry, McMeekin, Stokes, & Chandler, 1983):

$$\sqrt{k} = b(T - T_{\min})\left(1 - e^{c(T - T_{\max})}\right) \tag{10c}$$

All parameters in (10c) are defined as in (10b); $T_{\max}$ is the maximum temperature beyond which microbial growth does not occur. Ross and McMeekin (1994) cite several possible modifications:

$$\sqrt{k} = b(T - T_{\min})\sqrt{a_w - a_{w,\min}} \tag{10d}$$

$$\sqrt{k} = b(T - T_{\min})\sqrt{\mathrm{pH} - \mathrm{pH}_{\min}} \tag{10e}$$

$$\sqrt{k} = b(T - T_{\min})\sqrt{a_w - a_{w,\min}}\sqrt{\mathrm{pH} - \mathrm{pH}_{\min}} \tag{10f}$$

The parameter a_w is the water activity and $a_{w,\min}$ is the minimum water activity needed for microbial growth. This author would propose the following general form of equations (10a) to (10f):

$$b^n = \frac{k}{(T - T_{\min})^n} \frac{1}{(1 - e^{c(T - T_{\max})})^n} \prod_i (Q - Q_{\min})_i \tag{10g}$$

The variable ***Q*** is some quantity that affects cell growth, and $Q_{\min}$ is the minimum amount below which cell growth does not occur.

2.1.5 Arrhenius models

Ross and McMeekin (1994) state that the simplest Arrhenius model used is the equation itself:

$$\ln k = \ln A - \frac{E_a}{RT} \tag{11a}$$

The growth rate is ***k***, E_a is the characteristic temperature, ***R*** is the gas constant, ***T*** is the temperature and ***A*** is the model parameter. There are large deviations between observed and predicted behaviour at high and low temperatures using this simple model, which is to be expected since the Arrhenius equation describes reactions between elementary particles and not complex bacterial growth processes (Ratkowsky et al., 1982). More complicated models have since been proposed. One such example is the Schoolfield model (Schoolfield, Sharpe, & Magnuson, 1981):

$$\mathrm{r}(T) = \frac{\rho_{25^{\circ}\mathrm{C}} \frac{T}{298} \exp\left(\frac{\Delta H_A^{\neq}}{R}\left(\frac{1}{298} - \frac{1}{T}\right)\right)}{1 + \exp\left(\frac{\Delta H_L}{R}\left(\frac{1}{T_{0.5,\mathrm{L}}} - \frac{1}{T}\right)\right) + \exp\left(\frac{\Delta H_H}{R}\left(\frac{1}{T_{0.5,\mathrm{H}}} - \frac{1}{T}\right)\right)} \tag{11b}$$

The parameter $\mathrm{r}(T)$ is the known as the "mean development rate" as a function of temperature ***T***, ***R*** is the universal gas constant, $\rho_{25^{\circ}\mathrm{C}}$ is the rate at $25^{\circ}\mathrm{C}$ with 100% enzyme activation, $\Delta H_A^{\neq}$ is the activation enthalpy of the enzyme-catalysed reaction, ΔH_L and ΔH_H are the inactivation enthalpies associated with low temperatures and high temperatures respectively, and $T_{0.5,\mathrm{L}}$ and $T_{0.5,\mathrm{H}}$ are the temperatures at which 50% of the enzyme is inactivated by low and high temperatures respectively. This author feels the fact that this is a highly nonlinear equation raises serious concerns about the difficulty in fitting this model to data, since iterative regression techniques would have to be applied. These procedures produce parameter estimates which tend to converge to their true values only if "good" initial estimates are chosen as a starting point. Further, in working with novel halophilic strains it is unlikely

there would be enough data on the key growth-controlling enzymes from which values of the various enzyme constants could be deduced.

2.1.6 The model of Davey (1989)

Ross and McMeekin (1994) reports that a multi-linear model was provided by Davey (1989):

$$\ln k = C_0 + \frac{C_1}{T} + \frac{C_2}{T^2} + C_3 a_w + C_4 {a_w}^2 \tag{11c}$$

The model parameters are C_i for $i = 1, 2, 3, 4$. The other parameters have their usual meanings: ***k*** is the growth rate, ***T*** is temperature and a_w is the water activity. This model is notable for not being dependent on intrinsic microbial characteristics. The Arrhenius-like nature of this model stems from the reciprocals of ***T*** in conjunction with the natural logarithm and could thus be interpreted as a simpler alternative to the aforementioned Schoolfield model. This author would propose a generalisation and an extension to the Davey model:

$$\ln k = C_0 + \sum_{i=1} \left(\frac{A_i}{T^i} + B_i {a_w}^i + C_i [\mathrm{NaCl}]^i \right) \tag{11d}$$

The additive term represents a Taylor approximation to the effect of sodium chloride in the environment. The parameters A_i, B_i and C_i are to be found, and $[\mathrm{NaCl}]$ is the concentration of sodium chloride.

2.1.7 Response surface models

Ross and McMeekin (1994) provide a quadratic multi-linear regression model as an example. This author provides below the general form. Response surface models are ***N***-nomial regression models of the form:

$$y = \sum_{k=1}^{M_{C_N}} \left(b_k \prod_{j=1}^{M} {x_j}^{p_j} \right), \quad \text{where } \sum_{j=1}^{M} p_j = N \text{ and } M_{C_N} = \frac{M!}{N!\,(M-N)!} \tag{12}$$

The parameter ***y*** is known as the predicted variable and ***x*** as the explanatory variable. These models are empirical and are not built on any mechanistic understanding of actual underlying physiological processes.

2.1.8 Probability models

In their studies of staphylococcal growth in laboratory media (Genigeorgis, Martin, Franti, & Riemann, 1971), Genigeorgis *et al*. proposed an interesting kinetic model that is probabilistic. The probability of one cell dividing is:

$$P = \frac{R_D}{R_I} \tag{13a}$$

The parameter R_D is the number of cells that are dividing and R_I is the number of cells inoculated. The authors then proposed a quadratic multi-linear relationship between the number of decimal reductions $\log(R_I/R_G)$ and the pH and salt concentration in the media:

$$\log\frac{R_I}{R_D} = a + b_1[\%\mathrm{NaCl}] + b_2[\mathrm{pH}] + b_3[\%\mathrm{NaCl}]^2 + b_4[\mathrm{pH}]^2 + b_5[\mathrm{pH}][\%\mathrm{NaCl}] \tag{13b}$$

This is a quadratic multi-linear relationship that can be generalised in the same manner as in equation (12) and perhaps extended by introducing other factors e.g. phosphate levels, organic nitrogen availability and dissolved oxygen concentration. The idea of probabilistic modelling is supported by Ross and McMeekin (1994) who note that growth rates are highly variable when cell populations are exposed to conditions at the growth/no-growth boundary and other stressful conditions.

2.2 Hydrodynamic effects

2.2.1 Analytical solutions from theoretical considerations without reactions

There are fundamentally 2 different types of flow regimes: complete mixing (CM) and plug flow (PF). In an ideal completely mixed regime, the input constituents are immediately and uniformly dispersed throughout the flow domain upon entering. In the ideal plug flow regime, the exact opposite is true – fluid that enters the flow domain retains its structure and moves as

a single plug. Plug flow conditions can be achieved in a narrow long domain or in a flow domain with multiple baffles placed perpendicular to the predominant flow direction (Droste, 1997b). This is in fact the design chosen for the CFD mesh to be used in numerical simulations, where 4 baffles were placed perpendicular to the flow direction. Therefore one would expect the PF flow regime to dominate. In the presentation of analytical solutions below, the predominant flow direction is the x-direction.

2.2.1.1 Plug flow

Since fluid moves through the flow domain as a series of plugs, the mass balance equation cannot be written for the entire domain but only for an elemental volume (Droste, 1997b):

$$\big(QC - Q(C + \delta C)\big)\delta t + C_S \delta t = \delta V \delta C$$

Since $C_S = 0$ as before, this reduces to $-Q\delta C = A\delta x\left(\frac{\delta C}{\delta t}\right)$. This gives $-v\frac{\partial C}{\partial x} = \frac{\partial C}{\partial t}$. Since $v = {Q}/{A} = {\partial x}/{\partial t}$, we have $-\frac{\partial C}{\partial t} = \frac{\partial C}{\partial t}$. This is only possible if ${\partial C}/{\partial t} = 0$ i.e. the tracer concentration is invariant with time, as expected (Tchobanoglous, Burton, & Stensel, 2004b). The task now is to find the constant that describes $C(x,t)$, and this can be done by taking the Laplace transforms in the time domain (Droste, 1997a):

$$\mathcal{L}\left(-v\frac{\partial C}{\partial x}\right) = \mathcal{L}\left(\frac{\partial C}{\partial t}\right)$$

$$-v\frac{d\mathcal{C}}{dx} = s\mathcal{C}$$

The function $\mathcal{C} = \mathcal{L}(C)$ is independent of time t and s is the Laplace domain variable. This first-order ordinary differential equation is solved to give $\mathcal{C} = \mathcal{k}e^{-{xs}/{v}}$. The constant $\mathcal{k}$ can be found at $x = 0$ for a constant injection of a conservative tracer i.e. step input $C(0,t) = C_0\mathcal{K}(t-\tau)$. The tracer is injected at some time $\tau \geq 0$. Taking Laplace transforms:

$$\mathcal{C}(0,s) = C_0\frac{e^{-s\tau}}{s}$$

Therefore $C_0\frac{e^{-s\tau}}{s} = \mathcal{k}$:

$$\therefore \mathcal{C} = C_0 \frac{e^{-s\tau}}{s} e^{-xs/v} = C_0 \frac{\exp\left[-s\left(\tau + \frac{x}{v}\right)\right]}{s}$$

Taking the inverse transform gives an expression for the form of C:

$$C = \mathcal{L}^{-1}(\mathcal{C}) = C_0 \mathcal{K}\left(t - \left(\tau + \frac{x}{v}\right)\right) = \begin{cases} C_0 & t \geq \tau + \frac{x}{v} \\ 0 & t < \tau + \frac{x}{v} \end{cases}$$

This shows that the tracer concentration remains constant in the interval $x \in [0,\ vt - v\tau]$. A close inspection reveals that it is the nature of the partial differential equation governing the plug flow regime that preserves the form of the Laplace and inverse Laplace transforms. It is possible to model the effects of axial dispersion in a plug flow regime by using Fick's first law of diffusion $J = -D_{\text{eff}} \frac{\partial C}{\partial x}$. The diffusive flux J is taken to be directly proportional to the effective diffusion coefficient D_{eff}, which incorporates the effects of molecular diffusion and macroscopic turbulent diffusion. The mass balance for an elemental volume fluid in the plug flow regime becomes:

$$[(QC + AJ|_x) - (Q(C + \delta C) + AJ|_{x+\delta x})]\delta t + C_S \delta t = \delta V \delta C$$

The cross-section area is $A = {}^{V}/_{\delta x} = {}^{Q}/_{(\delta x/\delta t)}$, and the fluxes are defined as:

$$J|_x = -D_{\text{eff}} \frac{\partial C}{\partial x} \text{ and } J|_{x+\delta x} = -D_{\text{eff}} \frac{\partial}{\partial x}(C + \delta C)$$

Again $C_S = 0$, therefore:

$$-D_{\text{eff}} \frac{\partial C}{\partial x} A - Q\delta C - D_{\text{eff}} \frac{\partial}{\partial x}(C + \delta C)A = \delta V \frac{\delta C}{\delta t}$$

$$-v \frac{\partial C}{\partial x} - D_{\text{eff}} \frac{\partial^2 C}{\partial x^2} = \frac{\partial C}{\partial t}$$

The fact that $v = \delta x/\delta t$ gives:

$$\therefore \frac{\partial C}{\partial t} = -\frac{1}{2} D_{\text{eff}} \frac{\partial^2 C}{\partial x^2}$$

For a unit pulse input and small axial dispersion, this equation has the non-dimensional solution (Tchobanoglous, Burton, & Stensel, 2004c):

$$C_\theta = \frac{1}{2\sqrt{\pi D_{\text{eff}}/vL}} \exp\left(-\frac{(1-\theta)^2}{4D_{\text{eff}}/vL}\right)$$

This is in other words the impulse response. The parameter C_θ is the non-dimensional concentration C/C_0 where C_0 is the input tracer concentration, θ is the non-dimensional time t/t_d where t_d is the fluid detention time and L is the characteristic diffusion length-scale. This author would derive the step response from this impulse response. The step response is the integral of this impulse response:

$$C_\theta = \mathcal{K} + \frac{1}{2\sqrt{\pi}} \int_0^\eta \exp\left(-\frac{\eta^2}{4}\right) d\eta$$

The substitution $\eta = (\theta - 1)/\sqrt{D_{\text{eff}}/vL}$ was made, hence $d\eta = d\theta/\sqrt{D_{\text{eff}}/vL}$. The constant of integration can be found as:

$$C_\theta(t = +\infty) = \frac{C_\infty}{C_0}$$

$$\frac{C_\infty}{C_0} = \mathcal{K} + \frac{1}{2\sqrt{\pi}} \int_0^\infty \exp\left(-\frac{\eta^2}{4}\right) d\eta$$

$$\frac{C_\infty}{C_0} = \mathcal{K} + \frac{\sqrt{\pi}}{2\sqrt{\pi}}$$

$$\therefore C_\theta = \left(\frac{C_\infty}{C_0} - \frac{1}{2}\right) + \frac{1}{2\sqrt{\pi}} \int_0^\eta \exp\left(-\frac{\eta^2}{4}\right) d\eta$$

This corresponds to the non-ideal response curve shown in Figure G-4(b) of Tchobanoglous & Burton (1991) for continuous input.

2.2.1.2 Complete mixing

The mass balance equation for a flow domain receiving a constant input of conservative tracer at concentration C_0 for all time $t \geq 0$ is (Droste, 1997b):

$$Q(C_0 - C) + C_S = V\frac{dC}{dt}$$

The volumetric flow rate is Q, the tracer concentration at time t is C, the production rate of tracer in the volume V is C_S and the rate of change of C is $^{dC}/_{dt}$. Since the tracer is taken to be conservative, $C_S = 0$. This can be solved as a first-order separable equation, with the initial condition being that the concentration is described by a step function:

$$\int_0^C \frac{dC}{C_0 - C} = \int_0^t \frac{Q}{V} dt$$

$$C = C_0 - C_0 e^{-t/t_d}$$

The liquid detention time $t_d = {}^{V}/_{Q}$. Thus the tracer concentration C rises exponentially with the time constant t_d. If there are n fluid domains each of volume V/n connected in series and the dominant flow regime in each is complete mixing, then one may write the mass balance equation as (Tchobanoglous & Burton, 1991):

$$\frac{V}{n}\frac{d}{dt}C_2 = QC_1 - QC_2$$

Solutions to this equation for the concentration as a function of time in each of ***n***-CM reactors can be modelled numerically in MATLAB. The plots are presented in the Figure 1 below:

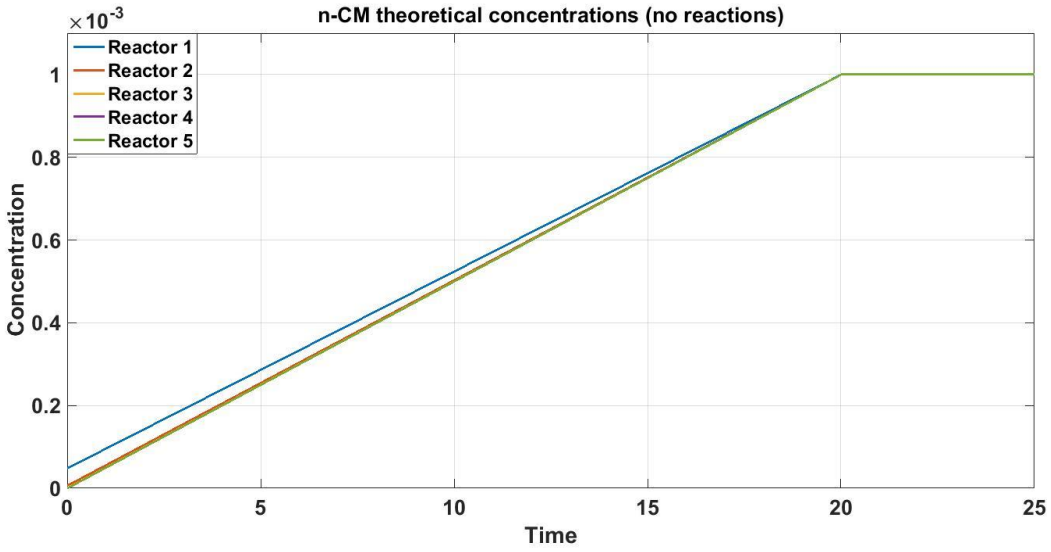

Figure 1: n-CM theoretical concentrations without reactions for n=5

2.2.2 Analytical solutions from theoretical considerations with reactions

In the previous section, the presentations of derivations did not include source terms. In this section changes in the concentration of a substance will be affected by its rate of production.

2.2.2.1 Plug flow

The mass balance equation is again:

$$\big(QC - Q(C + \delta C)\big)\delta t + C_S \delta t = \delta V \delta C$$

$$-v\frac{\partial C}{\partial x} + r_S = \frac{\partial C}{\partial t}$$

The volume source term $C_S = r_S A \delta x$ where r_S is the concentration rate term. The representative biochemical autocatalytic reaction implemented in the CFD simulations is:

$$\mathrm{C_5H_7O_2N} + \mathrm{C_{12}H_{22}O_{11}} + \mathrm{CON_2H_4} \rightarrow 3\mathrm{CO_2} + 2\mathrm{H_2O} + 3\mathrm{C_5H_7O_2N} + 4\mathrm{H_2}$$

Therefore the rate law would be:

$$-\frac{\partial}{\partial t}[\mathrm{CON_2H_4}] = -\frac{\partial}{\partial t}[\mathrm{C_{12}H_{22}O_{11}}] = \frac{\partial}{\partial t}[\mathrm{C_5H_7O_2N}]$$
$$= k_R[\mathrm{CON_2H_4}]^{\mathcal{A}}[\mathrm{C_{12}H_{22}O_{11}}]^{\mathcal{B}}[\mathrm{C_5H_7O_2N}]^{\mathcal{C}}$$

The reaction orders $\mathcal{A}$, $\mathcal{B}$ and $\mathcal{C}$ are empirical constants that do not need to be specified in the simulation input. Combining the rate law with the mass balance equation gives a set of 3 coupled partial differential equations:

$$-v\frac{\partial[\mathrm{CON_2H_4}]}{\partial x} - k_R[\mathrm{CON_2H_4}]^{\mathcal{A}}[\mathrm{C_{12}H_{22}O_{11}}]^{\mathcal{B}}[\mathrm{C_5H_7O_2N}]^{\mathcal{C}} = \frac{\partial[\mathrm{CON_2H_4}]}{\partial t}$$

$$-v\frac{\partial[\mathrm{C_{12}H_{22}O_{11}}]}{\partial x} - k_R[\mathrm{CON_2H_4}]^{\mathcal{A}}[\mathrm{C_{12}H_{22}O_{11}}]^{\mathcal{B}}[\mathrm{C_5H_7O_2N}]^{\mathcal{C}} = \frac{\partial[\mathrm{C_{12}H_{22}O_{11}}]}{\partial t}$$

$$-v\frac{\partial[\mathrm{C_5H_7O_2N}]}{\partial x} + k_R[\mathrm{CON_2H_4}]^{\mathcal{A}}[\mathrm{C_{12}H_{22}O_{11}}]^{\mathcal{B}}[\mathrm{C_5H_7O_2N}]^{\mathcal{C}} = \frac{\partial[\mathrm{C_5H_7O_2N}]}{\partial t}$$

The change in signs is due to the definition of r_S:

$$r_S|_{[\mathrm{CON_2H_4}]} = \frac{\partial}{\partial t}[\mathrm{CON_2H_4}], \quad r_S|_{[\mathrm{C_{12}H_{22}O_{11}}]} = \frac{\partial}{\partial t}[\mathrm{C_{12}H_{22}O_{11}}], \quad r_S|_{[\mathrm{C_5H_7O_2N}]} = \frac{\partial}{\partial t}[\mathrm{C_5H_7O_2N}]$$

Assume bacterial growth is first order i.e. $\mathcal{C} = 1$ and both urea and sucrose are in large excess i.e. zeroth-order $\mathcal{A} = \mathcal{B} = 0$. Then:

$$\mathcal{L}\left(-v\frac{\partial[\mathrm{C_5H_7O_2N}]}{\partial x} + k_R[\mathrm{C_5H_7O_2N}]\right) = \mathcal{L}\left(\frac{\partial[\mathrm{C_5H_7O_2N}]}{\partial t}\right)$$

Let $\mathcal{L}([\mathrm{C_5H_7O_2N}]) = \gamma$:

$$-v\frac{d\gamma}{dx} + k_R\gamma = s\gamma$$

$$\therefore \gamma = \hbar e^{-x(s-k_R)/v}$$

Taking into account the initial conditions:

$$\gamma(0,s) = C_0\frac{e^{-s\tau}}{s} = \hbar$$

$$\therefore \gamma = C_0\frac{e^{-s\tau}}{s}e^{-x(s-k_R)/v} = C_0\frac{\exp\left[-s\left(\tau + \frac{x}{v}\right) + \frac{xk_R}{v}\right]}{s}$$

The new additional term xk_R/v is independent of s:

$$[\mathrm{C_5H_7O_2N}] = \mathcal{L}^{-1}(\gamma) = C_0\mathcal{K}\left(t - \left(\tau + \frac{x}{v}\right)\right)\exp\left(\frac{xk_R}{v}\right) = \begin{cases} C_0\exp\left(\frac{xk_R}{v}\right) & t \geq \tau + \frac{x}{v} \\ 0 & t < \tau + \frac{x}{v} \end{cases}$$

This gives first-order kinetics as expected for $\mathcal{C} = 1$ and also proves that the ideal plug flow no longer applies. Remembering that $-v\frac{\partial C}{\partial x} = -\frac{\partial C}{\partial t}$, it can also be written in general:

$$-\frac{1}{2}k_R[\mathrm{CON_2H_4}]^{\mathcal{A}}[\mathrm{C_{12}H_{22}O_{11}}]^{\mathcal{B}}[\mathrm{C_5H_7O_2N}]^{\mathcal{C}} = \frac{\partial[\mathrm{CON_2H_4}]}{\partial t} \neq 0$$

Hence it can also be immediately seen that when the r_S term is introduced, the plug flow regime ceases as expected for all time $t \geq 0$ and for all reaction orders $\mathcal{A}, \mathcal{B}, \mathcal{C} \in \mathbb{R}$ (there is a non-zero initial $[\mathrm{C_5H_7O_2N}]$ so as to enable the reaction to start). If axial dispersion is to be taken into account, then one simply adds the diffusive term. For example:

$$-k_R[\mathrm{CON_2H_4}]^{\mathcal{A}}[\mathrm{C_{12}H_{22}O_{11}}]^{\mathcal{B}}[\mathrm{C_5H_7O_2N}]^{\mathcal{C}} - D_{\mathrm{eff}|[\mathrm{CON_2H_4}]}\frac{\partial^2[\mathrm{CON_2H_4}]}{\partial x^2} = 2\frac{\partial[\mathrm{CON_2H_4}]}{\partial t}$$

The term $D_{\mathrm{eff}|[\mathrm{CON_2H_4}]}$ is the effective diffusivity for $[\mathrm{CON_2H_4}]$. If first-order bacterial growth kinetics is assumed:

$$k_R[\mathrm{C_5H_7O_2N}] - D_{\mathrm{eff}|[\mathrm{CON_2H_4}]}\frac{\partial^2[\mathrm{C_5H_7O_2N}]}{\partial x^2} = 2\frac{\partial[\mathrm{C_5H_7O_2N}]}{\partial t}$$

2.2.2.2 Complete mixing

The mass balance equation is:

$$Q(C_0 - C) + C_S = V\frac{dC}{dt}$$

$$\therefore \frac{1}{t_d}(C_0 - C) + r_S = \frac{dC}{dt}$$

The set of 3 coupled partial differential equations become:

$$\frac{[\mathrm{CON_2H_4}]_0 - [\mathrm{CON_2H_4}]}{t_d} - k_R[\mathrm{CON_2H_4}]^{\mathcal{A}}[\mathrm{C_{12}H_{22}O_{11}}]^{\mathcal{B}}[\mathrm{C_5H_7O_2N}]^{\mathcal{C}} = \frac{d[\mathrm{CON_2H_4}]}{dt}$$

$$\frac{[\mathrm{C_{12}H_{22}O_{11}}]_0 - [\mathrm{C_{12}H_{22}O_{11}}]}{t_d} - k_R[\mathrm{CON_2H_4}]^{\mathcal{A}}[\mathrm{C_{12}H_{22}O_{11}}]^{\mathcal{B}}[\mathrm{C_5H_7O_2N}]^{\mathcal{C}} = \frac{d[\mathrm{C_{12}H_{22}O_{11}}]}{dt}$$

$$\frac{[\mathrm{C_5H_7O_2N}]_0 - [\mathrm{C_5H_7O_2N}]}{t_d} + k_R[\mathrm{CON_2H_4}]^{\mathcal{A}}[\mathrm{C_{12}H_{22}O_{11}}]^{\mathcal{B}}[\mathrm{C_5H_7O_2N}]^{\mathcal{C}} = \frac{d[\mathrm{C_5H_7O_2N}]}{dt}$$

If first-order bacterial growth kinetics and zero-order kinetics in the substrates are assumed, then the 3 coupled equations reduce to a single first-order differential equation:

$$\frac{[\mathrm{C_5H_7O_2N}]_0 - [\mathrm{C_5H_7O_2N}]}{t_d} + k_R[\mathrm{C_5H_7O_2N}] = \frac{d[\mathrm{C_5H_7O_2N}]}{dt}$$

This is due to the fact that $[\mathrm{CON_2H_4}]_0 = [\mathrm{CON_2H_4}]$, $[\mathrm{C_5H_7O_2N}]_0 = [\mathrm{C_5H_7O_2N}]$ and so their respective derivatives are zero. Letting $[\mathrm{C_5H_7O_2N}] = \gamma$, the solution can be found using an integrating factor I:

$$\frac{d\gamma}{dt} + \left(\frac{1}{t_d} - k_R\right)\gamma = \frac{\gamma_0}{t_d}$$

$$I = \exp\left(\int \left(\frac{1}{t_d} - k_R\right) dt\right) = \exp\left[\left(\frac{1}{t_d} - k_R\right) t\right]$$

$$\gamma = \exp\left[-\left(\frac{1}{t_d} - k_R\right) t\right]\left[\frac{\gamma_0}{t_d}\frac{t_d}{1 - t_d k_R}\exp\left[\left(\frac{1}{t_d} - k_R\right) t\right] + \kappa\right]$$

The initial condition is:

$$\gamma_0 = \frac{\gamma_0}{t_d}\frac{t_d}{1 - t_d k_R} + \kappa$$

$$\kappa = \gamma_0 - \frac{\gamma_0}{t_d}\frac{t_d}{1 - t_d k_R} = -\frac{\gamma_0 t_d k_R}{1 - t_d k_R}$$

$$\therefore [\mathrm{C_5H_7O_2N}] = \frac{[\mathrm{C_5H_7O_2N}]_0}{1 - t_d k_R}\left[1 - t_d k_R \exp\left[-\left(\frac{1}{t_d} - k_R\right) t\right]\right]$$

This demonstrates first-order kinetics up to a limiting value of $\frac{[\mathrm{C_5H_7O_2N}]_0}{1 - t_d k_R}$. In the case of *n* flow domains connected in series each of volume V/n and in which complete mixing effects dominate, the mass balance equation reads:

$$\frac{V}{n}\frac{d}{dt}C_{i+1} = QC_i - QC_{i+1} + C_S|_{i+1}$$

Therefore:

$$\frac{V}{n}\frac{d}{dt}[\mathrm{CON_2H_4}]_{i+1} = Q[\mathrm{CON_2H_4}]_i - Q[\mathrm{CON_2H_4}]_{i+1} - \frac{V}{n}k_R[\mathrm{CON_2H_4}]_{i+1}{}^{\mathcal{A}}[\mathrm{C_{12}H_{22}O_{11}}]_{i+1}{}^{\mathcal{B}}[\mathrm{C_5H_7O_2N}]_{i+1}{}^{\mathcal{C}}$$

Under the same set of assumptions of first-order bacterial growth kinetics and zero-order substrate reactions, this equation reduces to:

$$\frac{V}{n}\frac{d}{dt}[\mathrm{C_5H_7O_2N}]_{i+1} = Q[\mathrm{C_5H_7O_2N}]_i - Q[\mathrm{C_5H_7O_2N}]_{i+1} + \frac{V}{n}k_R[\mathrm{C_5H_7O_2N}]_{i+1}$$

Solutions for the concentration as a function of time in each of ***n***-CM reactors can be modelled numerically in MATLAB. The plots are presented in the Figure 2 below (assumed first-order reaction in all reactants):

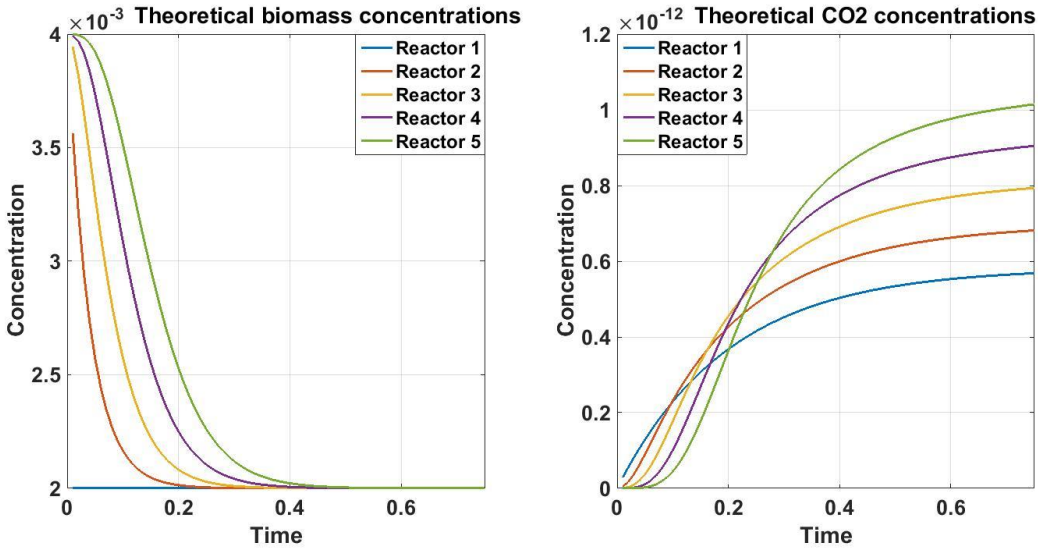

Figure 2: n-CM Theoretical biomass and CO2 concecntrations for n=5

3.0 Data and methods

3.1 Biological kinetic data model selection

Several models have been chosen based on 3 criteria: their extensibility, the expected computational effort and the amount of reference data needed. The extensibility of a model determines the ease with which additional parameters can be included, therefore the more extensible a model is, the more it is to be preferred. The expected computational effort is an important criterion; although nonlinear models tend to have a better numerical fit to data, many of them require computationally more expensive nonlinear regression for which convergence is not guaranteed. In the case of not being able to achieve numerical convergence, that effort is wasted. The amount of reference data needed determines the number of independent parameters that a model can have. There is in general a lack of published growth data on (novel) halophilic strains which implies that models with numerous tuneable parameters would be under-constrained. This leads to the problem of not being able to fix the values of the model coefficients. The application of the aforementioned criteria results in a preliminary list of candidate models: the model of Davey, the expanded cardinal model, the ***N***-order Tienungoon model and the Zwietering model.

3.1.1 The expanded cardinal model

Rosso *et al*. (1995) proposed the expanded cardinal model, which takes into account the minimum $x_{\min}$, maximum $x_{\max}$ and optimal x_{opt} values of the environmental parameter for bacterial growth. This model fixes the growth rate to be zero at both the minimum and maximum values of the environmental parameters, as can be seen from the form of the model below:

$$y = \frac{(x - x_{\min})(x - x_{\max})}{(x - x_{\min})(x - x_{\max}) - \left(x - x_{\text{opt}}\right)^2}$$

This author has modified this model to include 3 additional degrees of freedom by incorporating coefficients:

$$y = \frac{a(x - x_{\min})(x - x_{\max})}{b(x - x_{\min})(x - x_{\max}) - c\left(x - x_{\text{opt}}\right)^2}$$

This contains the original model as a special case where $a = b = c = 1$.

3.1.2 The *N*-order Tienungoon model

The original model (Tienungoon *et al.*, 2000) was:

$$y = (1 - 10^{x_{min} - x})(1 - 10^{x - x_{max}}) \qquad (2a)$$

This author has modified the original form to include additional degrees of freedom:

$$y = a\left(1 - B^{c(x_{min} - x)}\right)^N \left(1 - B^{b(x - x_{max})}\right)^N \qquad (2b)$$

This contains the original model as a special case where $B = 10$, a $= b = c = 1$, and $N = 1$. This author's choices were $B = e$ and to leave ***a***, ***b***, ***c*** and ***N*** as tuneable parameters. It should be noted that the choice of ***B*** not significant since ***b*** and ***c*** would absorb the difference.

3.1.3 The Zwietering model

Zwietering *et al*. (1990) proposed a model that would explicitly include the minimum, maximum and optimal values of the independent variable. This model is similar to the expanded cardinal model in that the growth response is fixed to be zero when the independent parameter is at

either the minimum or maximum value. Instead of being a proportion of linear functions as in the case of the expanded cardinal model however, the Zwietering model is a proportion of non-linear functions:

$$y = \left(\frac{(x - x_{\min})\left(1 - e^{b(x - x_{\max})}\right)}{\left(x_{\text{opt}} - x_{\min}\right)(1 - e^{b(x - x_{\max})})} \right)^2$$

Again this author has modified the original model to incorporate additional degrees of freedom by adding coefficients (contains the original model where $a = 1$ and $b = c$):

$$y = a\left(\frac{(x - x_{\min})\left(1 - e^{b(x - x_{\max})}\right)}{\left(x_{\text{opt}} - x_{\min}\right)(1 - e^{c(x - x_{\max})})} \right)^2$$

3.1.4 Data modelling

The growth data of *Haloanaerobium alcaliphilum*, a halophilic obligate anaerobe, was extracted from the several growth plots presented by Tsai *et al.* (TSAI et al., 1995). The growth rates of *H. alcaliphilum* at various concentrations of sodium chloride, at various pH conditions and at various temperatures were described. In each experiment, the amount of carbon macronutrient provided to the cells was in excess i.e. the carbon source was not a growth-limiting factor. In addition, the authors ensured that in each experiment only one environmental parameter was being altered and all the rest were kept constant. This allowed this author to deduce growth rate constants from the growth rate responses.

These datasets were then modelled using various functions in the Curve Fitting Toolbox® in Matlab® R2014b. All models used, with the sole exception of the Taylor approximation, were nonlinear models fitted to the data using the Trust Region algorithm which is "an improvement over the popular Levenberg-Marquardt algorithm" (Mathworks, 2014b). Bisquare weights were used to ensure robustness. 95% confidence intervals were calculated by the toolbox using the "inverse ***R*** factor […], the degrees of freedom for error, and the root mean squared error" (Mathworks, 2014a). Taylor approximations were also calculated and used as a standard reference against which the other models were compared. Taylor approximations were chosen as reference models because all infinitely differentiable functions have a Taylor representation,

and so this constitutes a common basis of comparison across different models. Though in principle a Taylor approximation can describe the data arbitrarily well given an arbitrarily high order, in itself a Taylor approximation indicates nothing of the underlying growth dynamics and so has not been used as an actual model.

The candidate models did not all perform well. Two additional criteria were further applied to select the best-performing kinetic models for the effect of each independent parameter on bacterial growth. First, the model with the highest R^2-statistic value was chosen because this implies that the numerical fit is the best. Second, the width of 95% confidence intervals must be of the same order of magnitude as the estimate itself. This second criterion ensures that the estimate has statistical significance. The application of these two criterion results in the selection of the model of Davey for modelling the effect of sodium chloride concentration and the ***N***-order Tienungoon model for modelling the effect of the other 2 variables.

3.1.4.1 Modelling the effect of sodium chloride concentration on the growth of *H. alcaliphilum*

4 models have been tested against the growth data of the halophile at various concentrations of sodium chloride: model of Davey, the expanded cardinal model, the *N*-order Tienungoon model and the Zwietering model. Out of the several models, the model of Davey appears to be the best: the residual sum-of-squares (RSS) is the lowest and the R^2-statistic is the highest. This can be seen in Table 1 below. The standard reference model has $RSS = 0.0023$ and $R^2 = 0.9551$.

Model	RSS	R^2
Model of Davey	0.002	0.9617
Expanded cardinal model	0.0025	0.9513
2-order Tienungoon model	0.0038	0.9275
Zwietering model	0.0043	0.9164
3-order Taylor approximation	0.0023	0.9551

Table 1: The RSS and R-squared statistics of various models for salt concentration

The third-order model of Davey was selected because it had the lowest RSS out of all models from order one to five with respect to the sodium chloride concentration. This can be seen in the Figure 3 below:

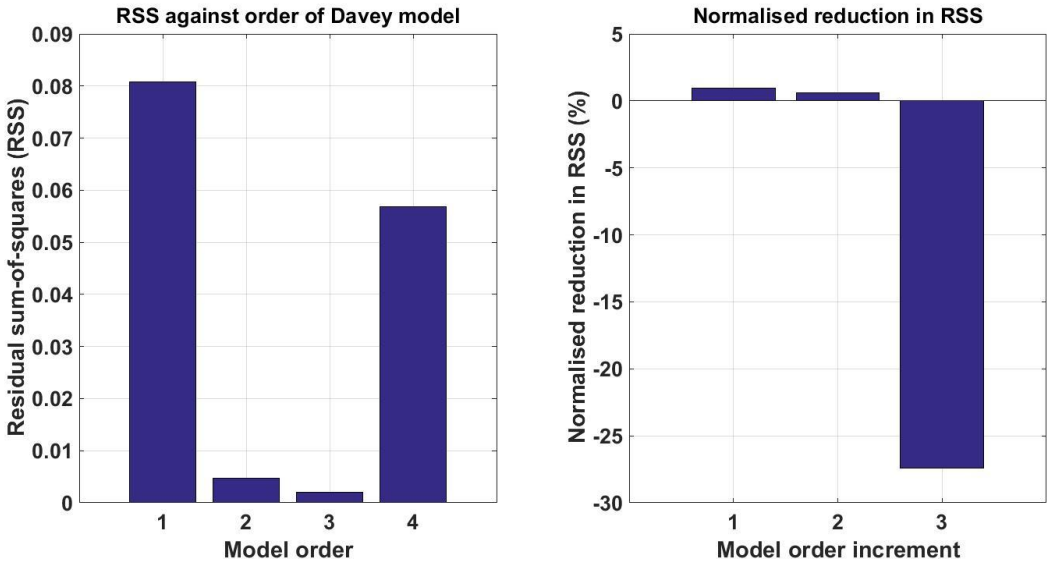

Figure 3: RSS plots for the model of Davey

The final positive normalised reduction in RSS occurred at the second order increment, after which the reduction became negative i.e. the RSS *increased*. Hence this justifies the choice of a third-order model of Davey. The second-order Tienungoon model was selected in this comparison because it has the lowest RSS out of all the ***N***-order Tienungoon models within the interval $1 \leq N \leq 5$. The order 5 was chosen as the upper limit of this interval because there are only 8 data points in total and the RSS of the Tienungoon models did not appear to be decreasing (see Figure 4 below).

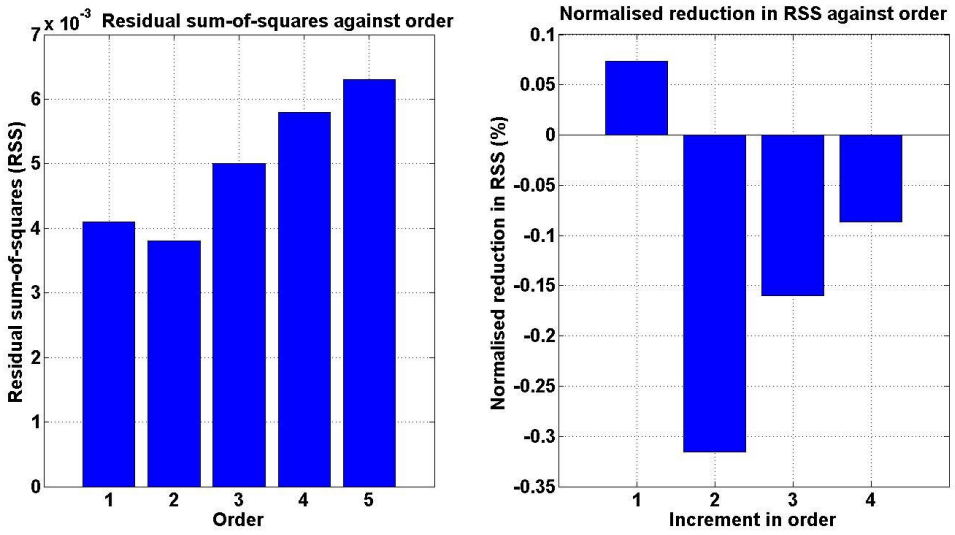

Figure 4: RSS plots for the Tienungoon models

After the first increment from a first-order to a second-order Tienungoon model, the normalised reduction in RSS became negative i.e. there is no return on the investment of additional computational effort in terms of model accuracy when increasing the model order (0.07317, -0.3158, -0.16, -0.08621). For similar reasons, a cubic Taylor approximation was chosen as the standard reference model; beyond the second increment the additional model complexity was not worth it, as can be seen from Figure 5 below. In this case, the model of Davey appears to be better than the reference model.

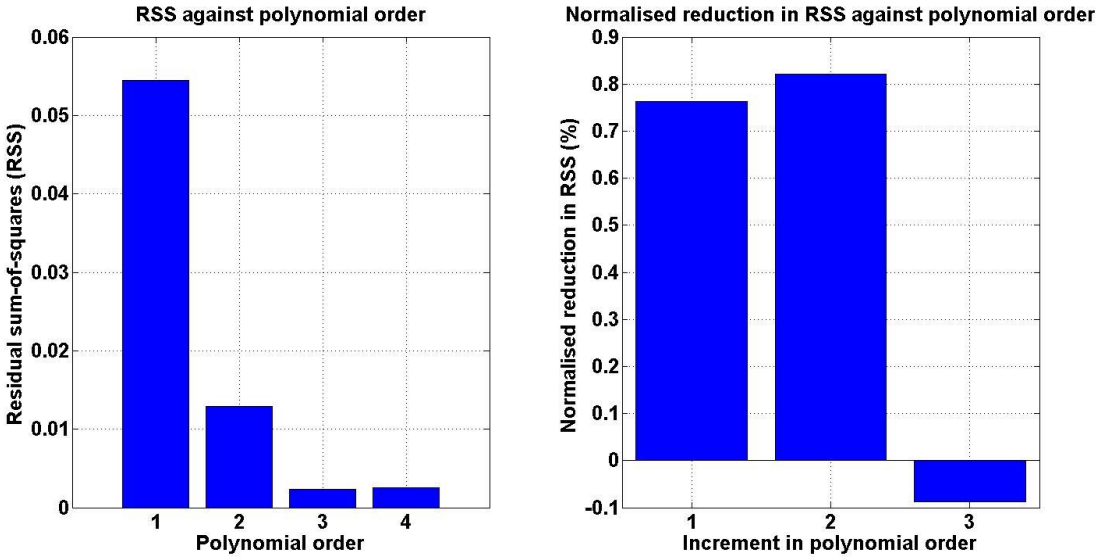

Figure 5: RSS plots for the reference model

The expanded cardinal model has a "good" R^2-statistic of 0.9513 and at first glance could have passed for a suitable model. Its basic statistics are shown in Table 2 below.

Coefficients	RSS	R^2
$a = 1.117 \in [-3 \times 10^7, +3 \times 10^7]$ $b = 4.761 \in [-1 \times 10^8, +1 \times 10^8]$ $c = 10.24 \in [-3 \times 10^8, +3 \times 10^8]$	0.0025	0.9513

Table 2: Coefficients and regression statistics for the expanded cardinal model

Upon closer inspection, a fundamental problem is revealed: the size of these intervals is about 8 orders of magnitude larger than the estimate itself – there is thus a large measure of uncertainty.

3.1.4.2 Modelling the effect of pH on the growth of *H. alcaliphilum*

The models which have been tested against the pH growth data are the expanded cardinal model, the *N*-order Tienungoon model and the Zwietering model. The 2-order Tienungoon model appears to be the "best" candidate, but it fares worse than the reference model, the R^2-statistic of which is 0.0115 higher and the RSS of which is 0.0029 lower. This can be seen in the Table 3 below.

Model	RSS	R^2
Expanded cardinal model	0.0259	0.8957
2-order Tienungoon model	0.0164	0.9340
Zwietering model	0.0638	0.7427
4th-order Taylor approximation	0.0135	0.9455

Table 3: The RSS and R-squared statistics of various models for pH

Both the Tienungoon and reference models have confidence intervals on the same order of magnitude as the estimate itself, which is reassuring. These confidence intervals are shown in the summary table at the end of this section. The 2nd-order Tienungoon model has the lowest RSS and the first increment gives a positive normalised reduction in RSS (though not the largest), which can be seen from the Figure 6 below. Thus it can be justified that the 2nd-order Tienungoon model is to be preferred over the others.

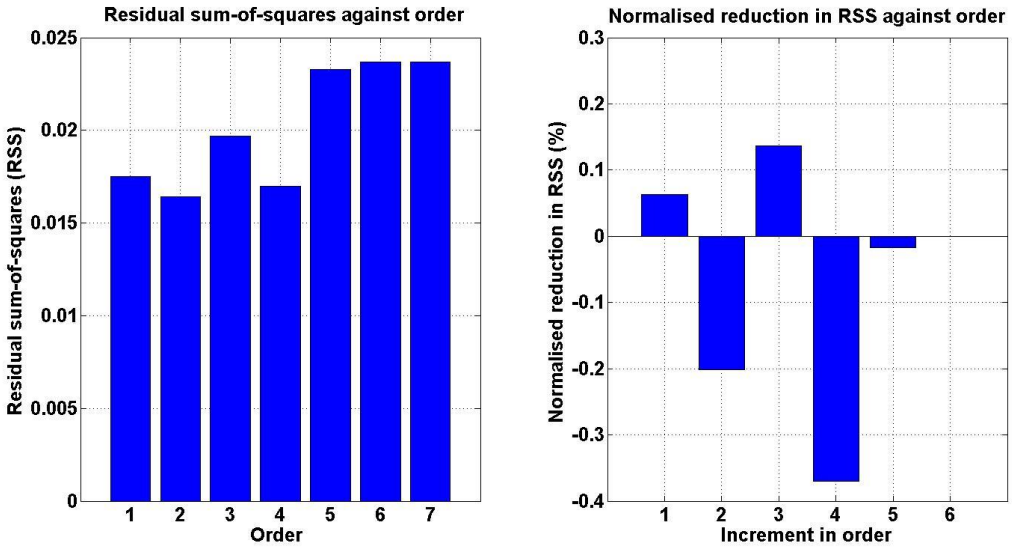

Figure 6: RSS plots for the 2nd-order Tienungoon model

In the same vein, the 4th-order Taylor approximation has the lowest RSS and the third increment is the last increment from which there is positive normalised reduction of the RSS, as can be seen from the Figure 7 below. Thus the choice of a 4th-order reference model is justified.

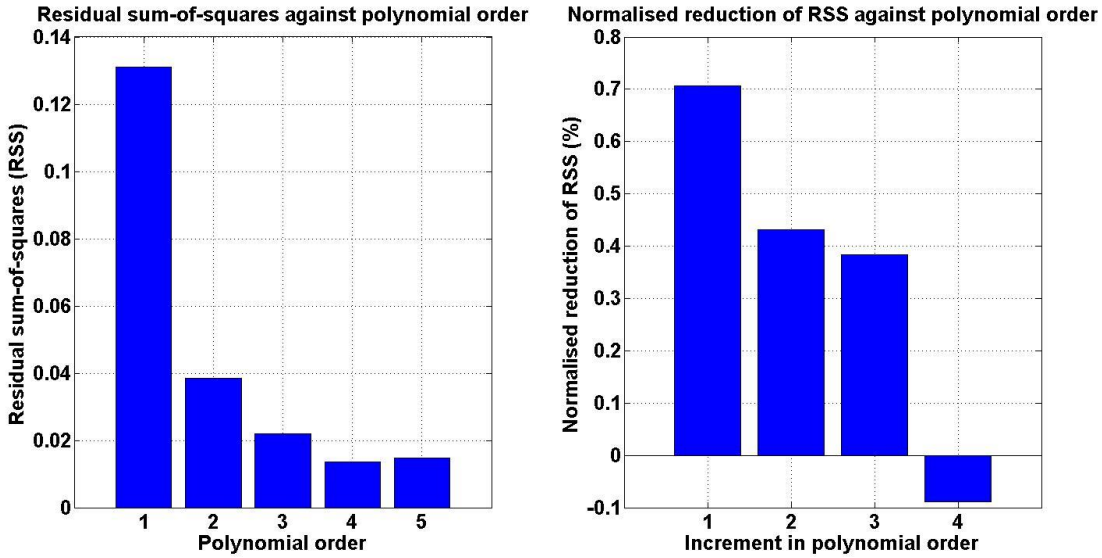

Figure 7: RSS plots for the reference model

3.1.4.3 Modelling the effect of temperature on the growth of *H. alcaliphilum*

The models which have been tested against the temperature growth data are the expanded cardinal model, the *N*-order Tienungoon model and the Zwietering model. Again it was found

that the generalised Tienungoon model gave the "best" match to the data, and in this case performed better than the reference model whose RSS is 0.0123 higher and whose R^2-statistic is 0.1208 lower. This can be seen from the Table 4 below.

Model	RSS	R^2
Expanded cardinal model	0.0074	0.9280
5th-order Tienungoon model	0.0042	0.9593
Zwietering model	0.0048	0.9532
2nd-order Taylor approximation	0.0165	0.8385

Table 4: Regression statistics of the various models for temperature

The 95% confidence intervals of the chosen model are again of the same magnitude as the estimates, and this assures that the parameter estimates have statistical significance. The confidence intervals for the 5th-order Tienungoon model are listed in the summary table. The RSS of the Tienungoon models stabilises at about 0.004 as the order increases to 7. This is corroborated by the fact that there is no normalised RSS reduction on the 6th increment, as can be seen from the Figure 8 below. Thus an order-5 Tienungoon model was selected.

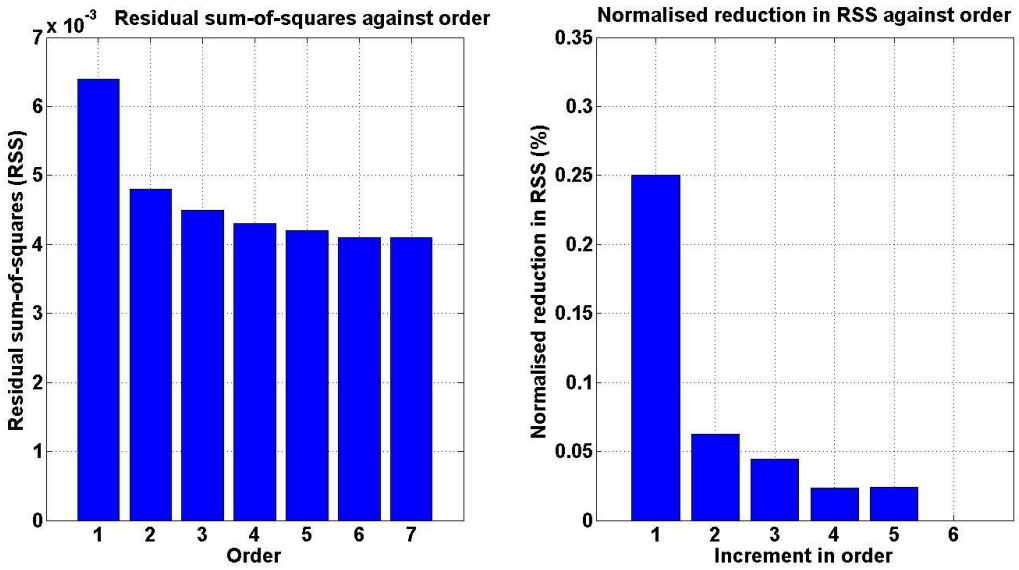

Figure 8: RSS plots of the 5th-order Tienungoon model

The RSS of various orders of the reference model are shown in the Figure 9 below. The greatest normalised reduction in RSS occurs in the first order increment. Thus a second-order Taylor

approximation was selected as a reference. It is not obvious to this author the reason for which there is a minimum in the variation of normalised reduction in RSS at the third order increment.

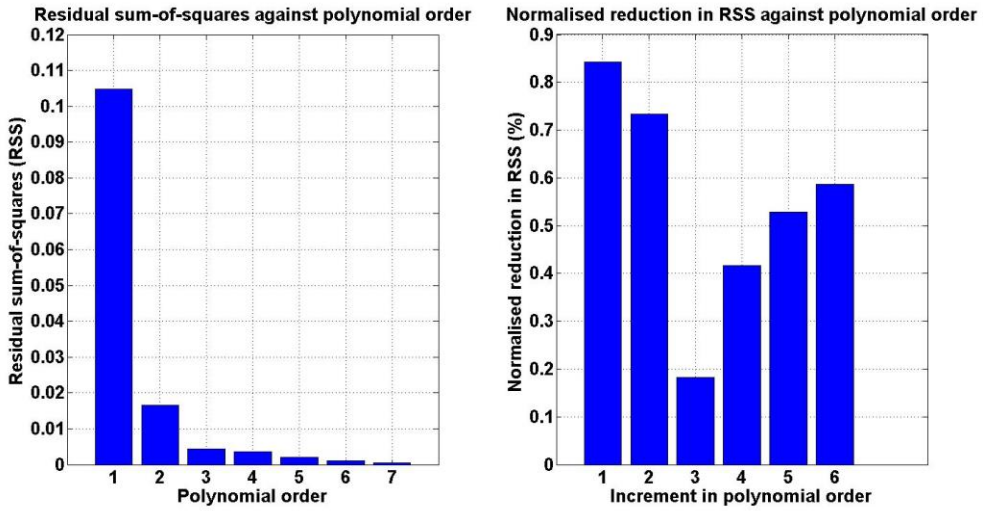

Figure 9: RSS plots of the reference model

3.1.4.4 Combined effects

The simplest approach would be to assume that the growth response to each and every environmental parameter is independent of the others and therefore multiply the 3 functions together, for example:

$$k_{\text{overall}} \propto \frac{k_{\text{temp}}}{k_{\text{temp, max}}} \times \frac{k_{\text{pH}}}{k_{\text{pH, max}}} \times \frac{k_{[\text{NaCl}]}}{k_{[\text{NaCl}], \text{max}}}$$

This is incorrect since amongst other things the heat response will modulate the other 2 responses. Growth responses to environmental circumstances are controlled by protein interactions which are strongly heat-dependent. Peterson *et al*. (2007) provides an example model of the effect of temperature on protein activity (equation 1). Therefore the true model would be more accurately written as:

$$k_{\text{overall}} \propto \text{k}(\text{pH}, \text{temp}) \times \text{k}([\text{NaCl}], \text{temp})$$

In the absence of additional published data describing the growth response as a function of multiple factors however, this might be the only approach available. A summary of the models chosen can be found in the Table 5 below.

Variable	Model	Form	Values & 95% confidence bounds	RSS	R^2
NaCl concentration	Davey	$y = e^{a+bx+cx^2+dx^3} + e$	$a = -1.291 \in [-7.804, 5.222]$ $b = 0.128 \in [-0.492, 0.749]$ $c = -0.008 \in [-0.048, 0.031]$ $d = 0.0001 \in [-0.0005, 0.0008]$ $e = -0.266 \in [-2.103, 1.570]$	0.0020 (0.0023)	0.9617 (0.9551)
pH	*N*-order Tienungoon	$y = a\left(1 - e^{c(x_{\min}-x)}\right)^n \left(1 - e^{b(x-x_{\max})}\right)^n$	$a = 0.354 \in [0.2906, 0.4174]$ $b = 1.323 \in [0.6474, 1.998]$ $c = 2.329 \in [0.9389, 3.718]$ $n = 2$	0.01637 (0.0135)	0.9340 (0.9455)
Temperature	*N*-order Tienungoon	$y = a\left(1 - e^{c(x_{\min}-x)}\right)^n \left(1 - e^{b(x-x_{\max})}\right)^n$	$a = 0.269 \in [0.218, 0.319]$ $b = 0.489 \in [0.304, 0.674]$ $c = 0.196 \in [0.135, 0.258]$ $n = 5$	0.0042 (0.0165)	0.9593 (0.8385)

Table 5: Summary of models selected

3.2 Computational Fluid Dynamics (CFD) simulations

CFD simulations were performed using the open-source freeware FreeFOAM, which is a branch variant ("fork") of OpenFOAM, where FOAM is an abbreviation for Field Operation And Manipulation. The decision to use an open-source CFD package was made because of cost considerations i.e. it is freeware, and the decision to use FreeFOAM instead of OpenFOAM in particular was made because FreeFOAM is much easier to install than OpenFOAM. FreeFOAM

needs no special shell scripts, does not depend on a large number of variables to run, and does not depend on a case-sensitive file system as does OpenFOAM (Wild & van der Graaf, 2012b). The file structure of a FreeFOAM simulation is shown in Wild & van der Graaf (2012b).

The default FreeFOAM installation comes with a wide variety of ready-to-use applications, utilities and libraries. A large number of routines known as *solvers* are provided in the installation, which can be used to solve fluid dynamics equations under different conditions. Regardless of the solver used, the file structure is the same, except that the set of `Properties` folders in the `constant` folder will be different. The <`time directories`> set of folders consists of one folder per time step, which in turn contains one sub-folder for each field variable being simulated. These are the outputs of the solver at each time step.

3.2.1 Mesh definition and generation

The governing partial differential equations for each problem case are to be solved on a discretised mesh. The CFD package utility *blockMesh* was used to generate a mesh that conforms to the geometry input by the user in the file `blockMeshDict`. The utility *blockMesh* generates a number of other data files based on this geometry input. The keyword `convertToMeters` is often set to unity, or sometimes increased so as to increase the cell sizes in the mesh. Cell sizes were sometimes adjusted to control the Courant number which cannot be larger than unity, for otherwise information is transmitted across a length-scale larger than the cell dimension in one time step. This implies that changes are not tracked properly from one cell to the next, making the numerical results unreliable. The nature of each face of the problem domain is specified in the `patches` section. Whilst multiple types of `patches` can be defined in FreeFOAM, only 3 types were ever used in CFD simulations: the generic `patch` (most commonly used to define inlets and outlets), the `wall` (used to define walls) and `empty` (used to define faces on which no solution is needed e.g. the faces of a 2-dimensional problem domain.

3.2.2 Initial conditions

Initial conditions can be found in the `0` folder in the main `case` directory – it is also the first in the set of *<time directories>*. One sub-folder is needed for each field variable being simulated. In all case studies considered so far, the pressure field `p` and the velocity field `U` were essential components regardless of solver used. The values of each field variable at $t = 0$ was represented in a text file.

3.2.3 Time control

An adaptive algorithm that adjusts the time step according to the value of the Courant number was used. By specifying a maximum Courant number `maxCo` and a maximum time step size `maxDeltaT`, the algorithm will maximise the time step as far as possible without the Courant number exceeding the set value. In this way excessively small time steps are avoided (which can result in output values that are indistinguishable from one another), as are time steps that are too large (which can result in numerical instability). After the completion of the simulation, the results were visualised in ParaView, which is an open-source data visualisation and analysis tool that is packaged together with the default installation of FreeFOAM. Screenshots and animations were produced using ParaView, plots were produced in MATLAB.

3.2.4 Solvers

The default FreeFOAM installation provides a large number of ready-to-use solver applications. For the purposes of this project, only a few were used: `ico`, `settling`, and `reacting`. The full list of solver applications provided in FreeFOAM can be found in the user guide (Wild & van der Graaf, 2012a).

3.2.5 Case studies

A number of CFD simulations were performed to investigate hydrodynamic effects and the combined effects of hydrodynamics and biological reactions. The purpose of performing these simulations was to compare the numerical results against analytical solutions to investigate deviations from theory and hence infer the circumstances under which the analytical solutions can and cannot be applied. These CFD simulations were performed on a mesh geometry shown

in Figure 10 below. For simplicity of comparison to analytical solutions, a 2-dimensional case was selected.

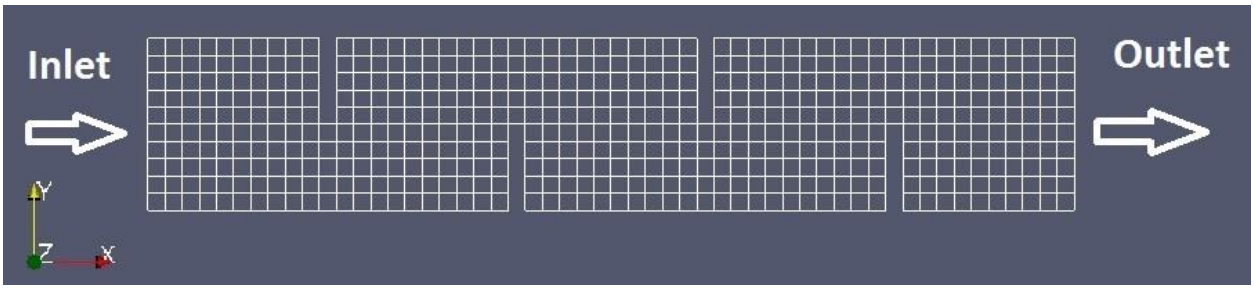

Figure 10: Mesh of test domain used in CFD simulations

This geometry describes a tank that can be used for the clarification of mixed liquor from an aeration basin. This geometry was chosen in order to study both hydrodynamic and biological effects in flows, and also because it is relatively simple to describe. Apart from the inlet and outlet, the rest of the problem domain surface is prescribed as walls. This will be modelled as a completely-mixed domain and as a plug flow domain. Since a non-ideal plug flow domain can be modelled as a series of completely-mixed reactors (Tchobanoglous et al., 2004c), this domain will be modelled as a series of 5 completely-mixed reactors corresponding to the 5 regions in between the baffles. In total, 4 CFD simulations were performed, some of which took into account biological reactions and some of which took into account density effects. These are summarised in the Table 6 below.

Simulation	Solver used	Biological reaction	Density effects
A	`settlingFoam`	No	No
B	`settlingFoam`	No	Yes
C	`reactingFoam`	Yes	No
D	`reactingFoam`	Yes	Yes

Table 6: List of simulations performed

3.2.5.1 Numerical simulation of pure hydrodynamic effects

The solver `settlingFoam` was used because it is able to simulate the settling of an immiscible dispersed phase within another phase. In particular, this solver solves the following equations (Wild & van der Graaf, 2012c):

The density continuity equation (density is ρ, the time t and the velocity vector field is $\widetilde{\boldsymbol{u}}$):

$$\frac{\partial \rho}{\partial t} + \nabla \cdot (\rho \tilde{\boldsymbol{u}}) = 0$$

The momentum conservation equation, also known as the Navier-Stokes (the effect of hydrostatic pressure due to gravity is accounted for separately in the equation $p = p_0 + \rho g h$ where p_0 is a reference pressure and h is the height from a reference baseline). The parameter $\phi = \rho \tilde{\boldsymbol{u}}$ and μ refers to the dynamic (shear) viscosity.

$$\frac{\partial}{\partial t}(\rho \tilde{\boldsymbol{u}}) + \nabla \cdot (\phi \tilde{\boldsymbol{u}}) + \nabla^2 (\mu \tilde{\boldsymbol{u}}) = 0$$

The solid fraction α evolution equation:

$$\frac{\partial}{\partial t}(\rho \alpha) + \nabla \cdot (\phi_\alpha \alpha) - \nabla \cdot (\mu \nabla \alpha) = 0$$

The parameter ϕ_α is a surface scalar field derived from the density of the non-settling phase, and μ is again the dynamic viscosity.

In the folder for initial conditions, the input file `alpha.txt` describes an initial uniform solid fraction distribution of zero throughout the domain, and a constant input of 0.001 at the inlet (i.e. a step input). The files `epsilon.txt` and `k.txt` describe the turbulent dissipation rate and the turbulent kinetic energy respectively. The file `p_rgh.txt` describes the pressure distribution and the file `U.txt` describes the velocity field.

3.2.5.2 Numerical simulation of hydrodynamic effects coupled with biological reactions

The solver `reactingFoam` was chosen because it is able to simulate chemical reactions and at the same time simulate fluid behaviour. Using this solver would therefore demand an appropriate method of representing the biological reactions in a solver that was originally designed to account only for traditional chemistry. The `reactingFoam` solver solves a number of equations, in particular (Wild & Graaf, 2012):

$$\frac{\partial}{\partial t}(\rho \tilde{\boldsymbol{u}}) + \nabla \cdot (\phi \tilde{\boldsymbol{u}}) + T = \rho g$$

The parameter ϕ is a surface scalar field interpolated from the density ρ and velocity $\widetilde{\boldsymbol{u}}$ fields. This equation accounts for the turbulence in the term T and density currents are also accounted for by the term ρg. The following equation is also solved:

$$\frac{\partial}{\partial t}(\psi p) + \nabla \cdot \phi + \nabla \cdot \rho r_{UA} \nabla p = 0$$

The parameter ψ is an internal thermodynamic variable, ϕ and ρ are defined as above, r_{UA} is a volume scalar field interpolated from the velocity field and p is the pressure.

In the folder for initial conditions, the file `T.txt` contains the initial and boundary field values for the temperature distribution. The file `C12H22O11.txt` contains the initial and boundary field values for the sucrose input, and similarly for the `CON2H4.txt` file, which contains data for the urea input. Both sucrose and urea are substrates for bacterial growth, and are injected in equal proportion to each other at a constant rate for time $t \geq 0$ i.e. step input. This is also the stoichiometric proportion, as can be seen from the representative bacterial growth reaction equation below:

$$\mathrm{C_5H_7O_2N} + \mathrm{C_{12}H_{22}O_{11}} + \mathrm{CON_2H_4} \rightarrow 3\mathrm{CO_2} + 2\mathrm{H_2O} + 3\mathrm{C_5H_7O_2N} + 4\mathrm{H_2}$$

The bacterial biomass is represented as $\mathrm{C_5H_7O_2N}$ (Rittmann & McCarty, 2001). This biochemical reaction incorporates urea as a nitrogen source and sucrose as a carbon source in the absence of oxygen, since *Haloanaerobium alcaliphilum* is an obligate anaerobe (Tsai et al., 1995). Bacterial biomass is produced as a consequence of a certain amount of bacterial biomass being already present *a priori*. This can be represented as an autocatalytic reaction using conventional notation in `FreeFoam`, which explains the presence of one unit of bacterial biomass on the left side of the above chemical equation. This reaction scheme and a full list of chemical species involved can be found in the `reactions.txt` file in the `constant` folder. Three rate constant parameter values are needed in the `reactions` file. The reaction rate constant k is defined as:

$$k = A_i T^{\beta_i} \exp\left(-\frac{E_i}{RT}\right)$$

The parameters are A_i, β_i and E_i where E_i is the activation energy for the reaction. If β_i is set to zero, A_i becomes the pre-exponential factor. These 3 parameters in FreeFOAM therefore provide the link to the biokinetics aspect of these bacterial-dependent reactions. The rate of a reaction r can be written as:

$$r = k \prod_i [R_i]^j$$

k is the rate constant defined above, $[R_i]$ is the concentration of the i-th reactant and j is the order of the reaction with respect to $[R_i]$. The rate of reaction as a function of several environmental variables has been previously modelled. The rate of this reaction is the bacterial growth rate, so the task now is to choose values for A_i, β_i and E_i for this reaction that will reflect the influence of environmental conditions on the bacterial growth rate. In the characterisation study performed by Tsai *et al*. (1995), the growth rates of *H. alcaliphilum* were evaluated across a range of pH values, temperatures and sodium chloride concentrations. When evaluating the bacterial growth response as a function of one environmental variable, the other 2 variables were kept constant at known values. The models that this author has applied to model these responses are models of growth rates. Under the (reasonable) assumption that growth substrates are not limiting, the reaction rate r becomes zeroth order with respect to the reactant concentrations and therefore r becomes k:

$$r = k[\mathrm{C_{12}H_{22}O_{11}}]^0[\mathrm{CON_2H_4}]^0 = k$$

Therefore it can be justified that the models are of the growth rate constant k itself. Each model provides a function for the rate constant, and the 3 functions need to be combined in some way to result in an overall rate constant that is a function of all 3 variables. This can be done by writing:

$$k_{\mathrm{overall}} = k_{\mathrm{pH}} \frac{k_{\mathrm{NaCl}}}{k_{\mathrm{NaCl,\,max}}} \frac{k_{\mathrm{temp}}}{k_{\mathrm{temp,\,max}}}$$

$k_{\mathrm{NaCl,\,max}}$ and $k_{\mathrm{temp,\,max}}$ are the maximum rate constants predicted by the models of the respective environmental variables. k_{overall} is therefore a double normalised form of k_{pH}; the reason k_{pH} was chosen as the base constant to normalised is simply because k_{pH} displays the

largest numerical range and so can capture the largest range of growth responses. Selecting a specific combination of values for the pH, temperature and sodium chloride concentration gives a specific value for k_{overall}, which can be equated to the exponential form of the reaction rate constant. This allows values of A_i, β_i and E_i to be chosen to match the values of k in both expressions, incorporating the effects of pH, temperature and sodium chloride concentration on the bacterial growth response. This has elected to set the sodium chloride concentration and the temperature to their optimal values such the respective normalising factors are each unity, and to set the pH to the optimal as well, which results in $k_{\text{overall}} = k_{\text{pH, max}} = 0.3454$. Taking $E_i = 25000$, $A_i = 2.155 \times 10^{13}$. In order to speed up what is a slow reaction, a factor of 60 was applied on the pre-exponential factor such that $A_i = 1.293 \times 10^{15}$.

The file `thermo.compressibleGas.txt` contains the thermochemical data for all the chemical species involved in the reaction. The molecular mass is first specified, followed by the temperature ranges over which the NASA 7-term polynomial coefficients are applicable. The last row contains the hard-coded constants $A_s = 1.67212 \times 10^{-6}$ and $T_s = 170.672$ used to calculate the laminar viscosity from Sutherland's law. The polynomial coefficients were obtained from simultaneous regression of multiple thermochemical properties (Mcbride, Gordon, & Reno, 1993) and thus can be used to model the values of these properties for use during the CFD simulation. However the values are provided as plaintext in their original form, and this makes usage inconvenient. Hence this author has decided to use an Excel workbook developed by Dr. Christos Samaras (Samaras, 2015) which draws upon the raw values stored in Prof. Burcat's database (Burcat, 2006). Thermochemical data for sucrose in the aqueous state could not be found, and because $\mathrm{C_5H_7O_2N}$ is a representative formula for bacterial biomass no actual data exists for this. Substitutes were therefore used. Since sucrose is a energy source for the growing cells, this author decided to use the data for *n*-heptanol instead because the heat of combustion of both substances is similar.

After the simulations were complete, data corresponding to the various field variables were sampled along a line of resolution 100 points running perpendicular to the predominant flow direction at each constriction caused by the presence of a baffle. This was done at every time

step using the FreeFOAM `sample` utility. The sampled datasets were processed by a number of MATLAB scripts to evaluate the root-mean-squared error (RMSE) between the theoretical predictions and the CFD results as a function of time. The RMSE therefore serves as a metric for the amount of deviation from theory and the RMSE profile in time provides information on the relative accuracy of theoretical predictions at various time points.

4.0 Comparing the simulated outputs with the analytical solutions

4.1 Comparing the results from simulation A with the analytical solutions for plug flow and complete mixing of a conservative neutrally buoyant tracer

The settling of the dispersed phase is shown in Figure 11 below:

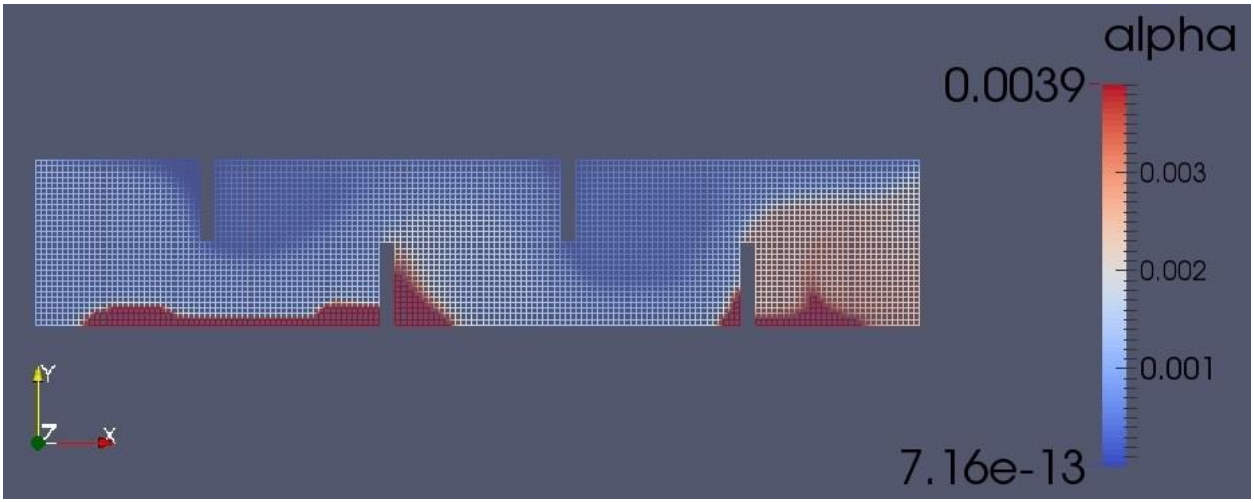

Figure 11: Settling of the dispersed phase in Simulation A

Plots of the root-mean-squared error (RMSE) of the numerical results compared to the analytic solutions are shown in the 2 Figures 12 and 13 below. The RMSE compared to the PF solution first increase, then drop slightly. With the notable exception of the RMSE corresponding to the first constriction which increases dramatically up to a plateau, the others achieve a relatively low and somewhat stable value.

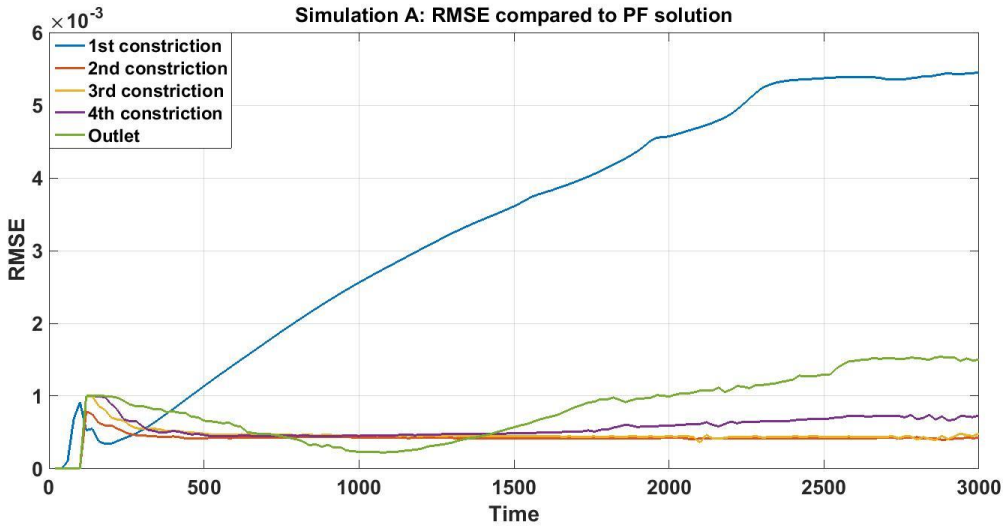

Figure 12: RMSE compared to PF solution (Simulation A)

A very similar set of trends was found in the RMSE values when the numerical results were compared to the CM solution. This suggests that therefore the ***n***-CM solution does indeed approximate the PF theoretical solution, but unfortunately neither describes the numerical solution well especially at the first constriction. It is perhaps important to note that the numerical solution does not converge to either the PF or CM solutions.

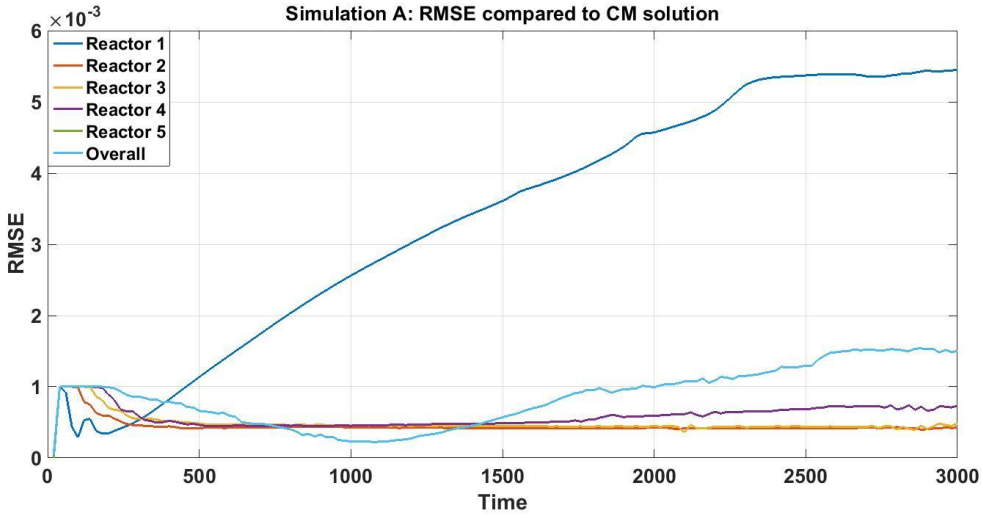

Figure 13: RMSE compared to CM solution (Simulation A)

4.2 Comparing the results from simulation B with the analytical solutions for plug flow and complete mixing of a conservative tracer that experiences density settling effects

A screenshot of the distribution of the dispersed phase is shown in the Figure 14 below:

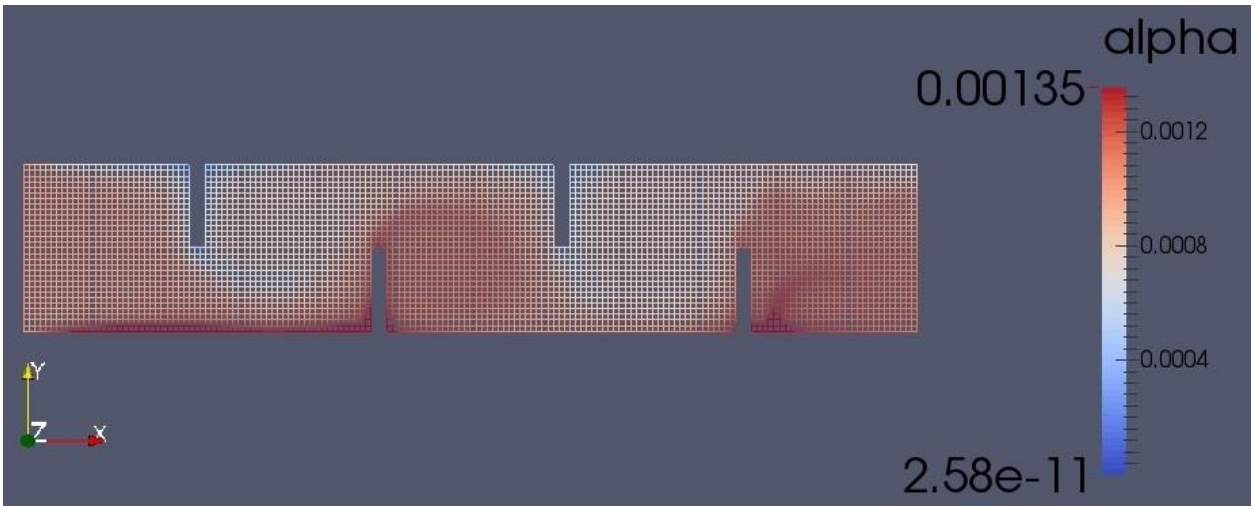

Figure 14: Settling of dispersed phase with density effects (Simulation B)

The RMSE values of the numerical solution compared to the PF solution exhibit large initial values and decays away with time in a seemingly exponential fashion (Figure 15). The RMSE values in general increase with the distance from the inlet i.e. the further the constriction is from the inlet the larger the deviations from the predicted flow. The RMSE values again decay away with time but without exception in this case. The RMSE values associated with those constrictions further away decayed more slowly. The largest magnitudes of the RMSE are still lower than those in Simulation A, which suggests that the presence of density settling effects improves the convergence of the numerical solution to the PF solution, although exact convergence was not achieved within the timeframe of the simulation.

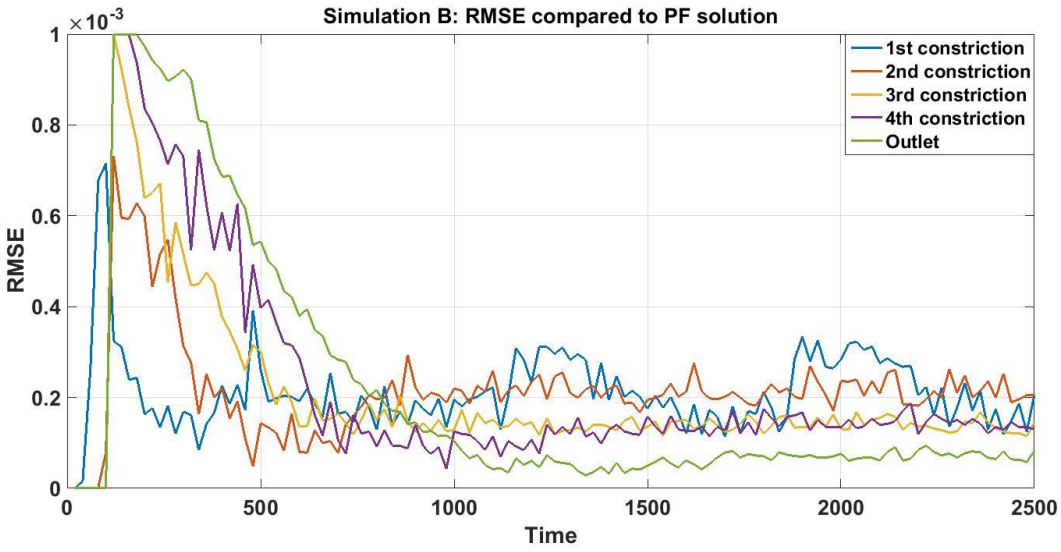

Figure 15: RMSE compared to PF solution (Simulation B)

The behaviour of the RMSE values when the numerical results are compared to the CM solution is similar (Figure 16), and suggests that in the case of flow with settling effects the ***n***-constriction PF solution matches the ***n***-reactor CM solution. It is notable that the RMSE values in Simulation B are a lot more oscillatory than those in Simulation A, despite identical initial and boundary conditions. This could be due to increased turbulence, and suggests that density currents have a significance impact on the flow regime not accounted for in either pure CM or PF models.

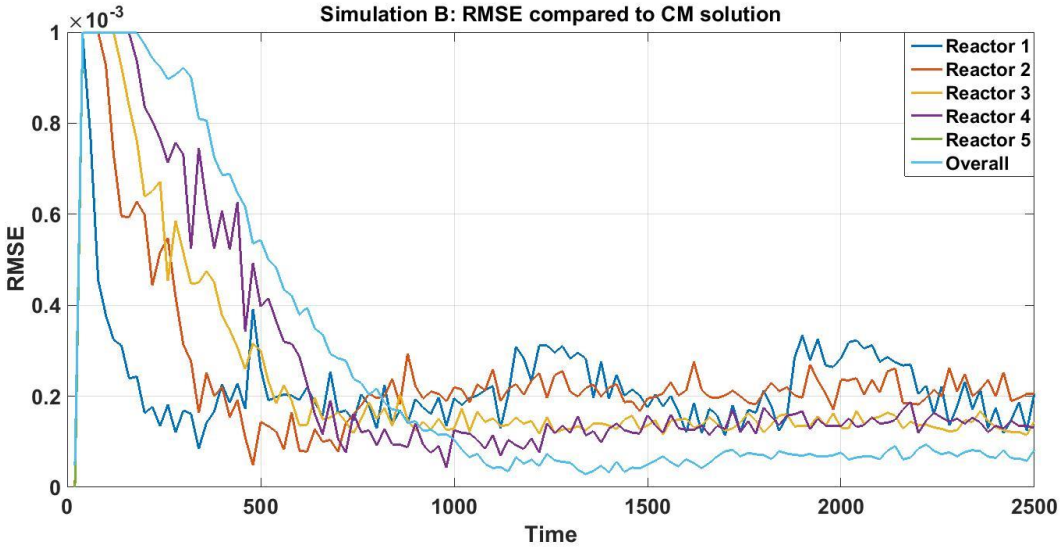

Figure 16: RMSE compared to CM solution (Simulation B)

4.3 Comparing the results from Simulation C with the analytical solutions for plug flow and complete mixing

Plots of the biomass and carbon dioxide concentrations from this Simulation C are shown in Figure 17 below, and are representative of those from Simulation D as well:

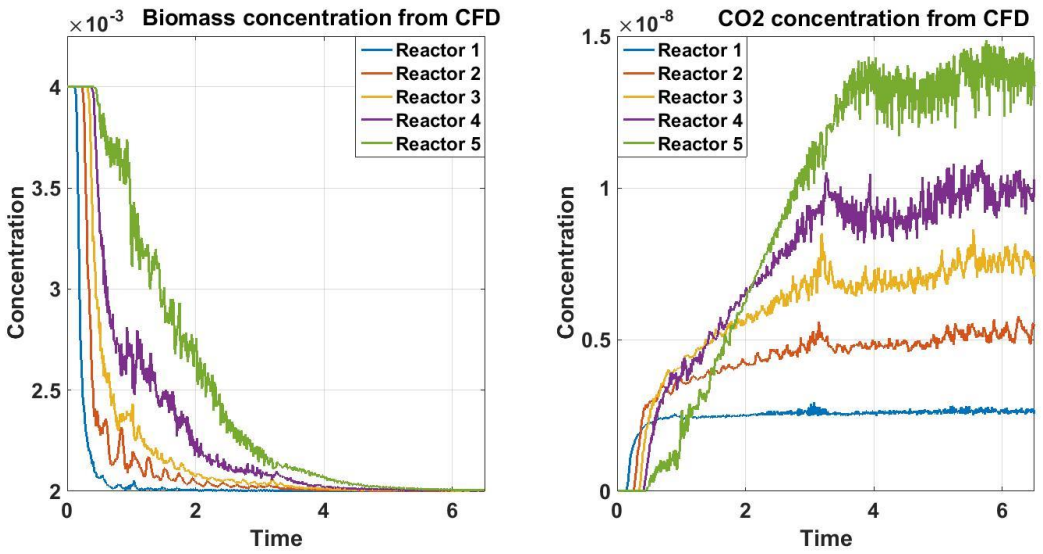

Figure 17: Biomass and carbon dioxide concentrations from Simulation C

A screenshot of the biomass concentration field distribution is shown in the Figure 18 below:

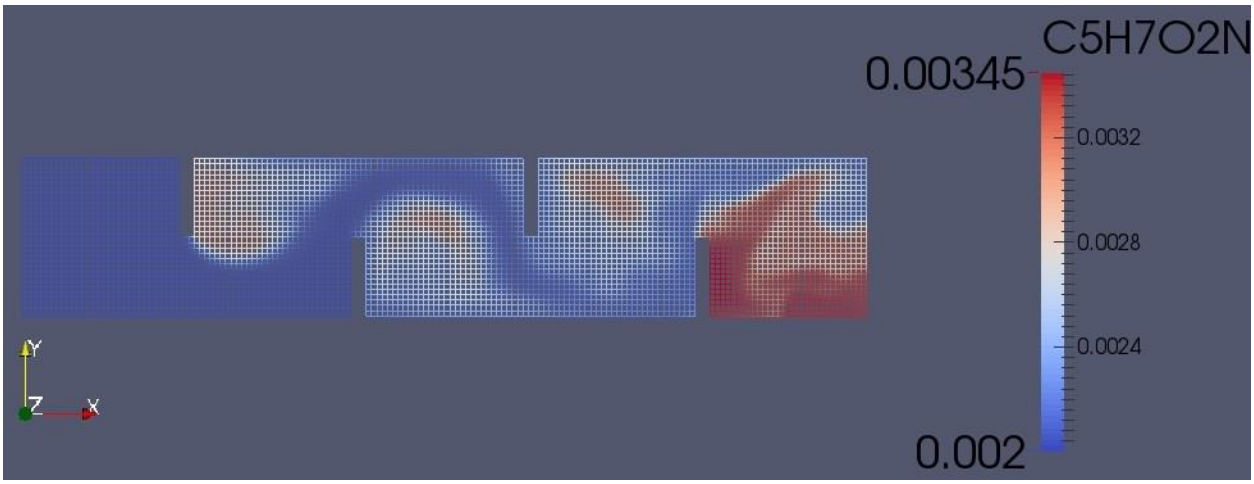

Figure 18: Biomass distribution in Simulation C

The biomass distribution clearly shows 4 regions of high mixing activity and a serpentine flow that is only slightly entrained into each of the 4 well-mixed regions. This suggests that an

approximate approach to modelling this flow domain could be to partition it into multiple CM reactors and to incorporate a PF contribution. This also validates the theoretical approach adopted here, which was to model this domain as a series of CM reactors. Simulation C takes into account the effect of biological reactions on the concentrations of various chemical species, in addition to modelling hydrodynamic effects. It can be seen that the RMSE values all decay to zero over a much shorter time-scale than in either Simulations A or B, but retains a similar behaviour in that the RMSE values associated with constrictions that are further are larger. Despite this, a much better convergence to the PF solution is observed, and oscillations are of a much higher frequency. Both indicate that biological reactions play a significant role in altering the flow regime.

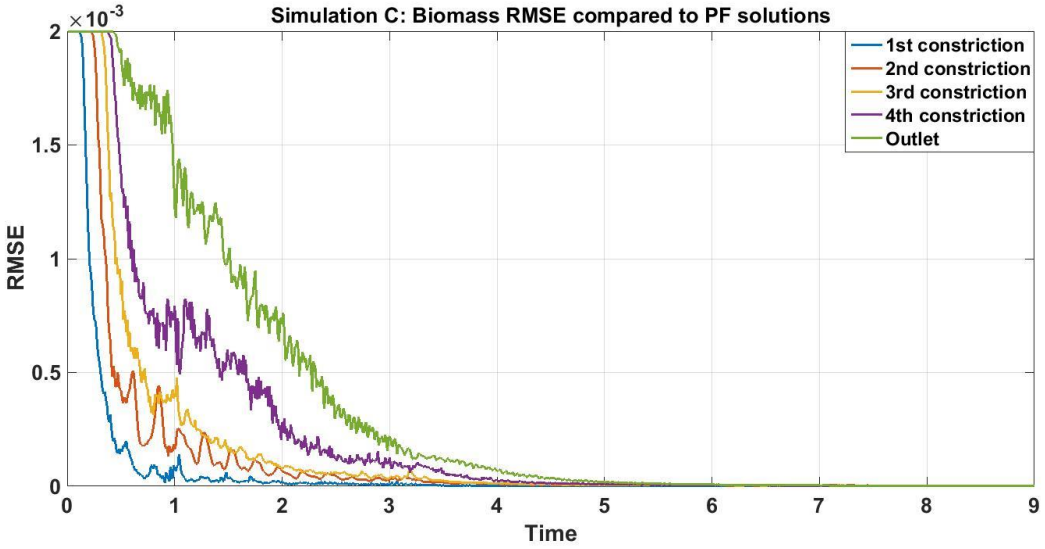

Figure 19: RMSE of biomass concentration compared to PF solutions

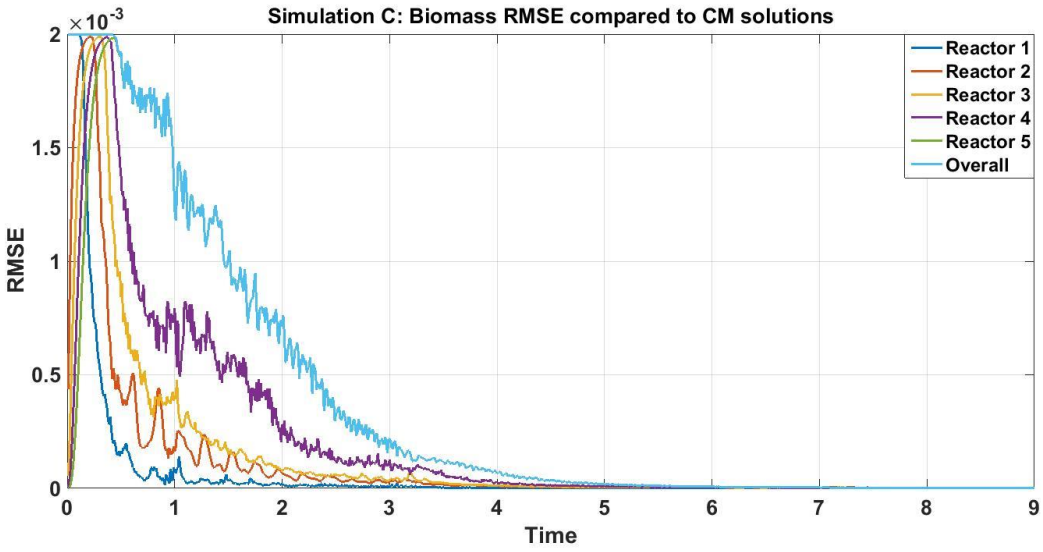

Figure 20: RMSE of biomass concentration compared to CM solutions

The RMSE values of the biomass numerical results compared to the CM solution exhibit a peak (Figure 20), unlike those associated with the PF solution (Figure 19). The further the reactor is from the inlet, the larger the time delay in the arrival of the RMSE peak, the larger the RMSE decay timescale, and the larger the RMSE values. Both sets of RMSE data suggest that pure CM and PF models are particularly inadequate for modelling transient effects, but may be suitable for modelling the steady-state flow regime in the presence of biological reactions. The RMSE plots for sucrose and urea with respect to PF and CM solutions are not shown due to a high degree of similarity with the preceding plots.

Screenshots of the carbon dioxide distribution is shown in the Figure 21 below (the left at $t = 1.1$ and the right at $t = 3.5$). It can be observed that the distribution of carbon dioxide also follows a similar pattern of 4 well-mixed regions and a PF component. The flow regime therefore plays a significant role in altering biological kinetics. Since the concentration of carbon dioxide is taken to be a proxy for biological activity then most of the substrate-to-biomass conversion takes place only in the well-mixed regions and not in the serpentine plug flow region.

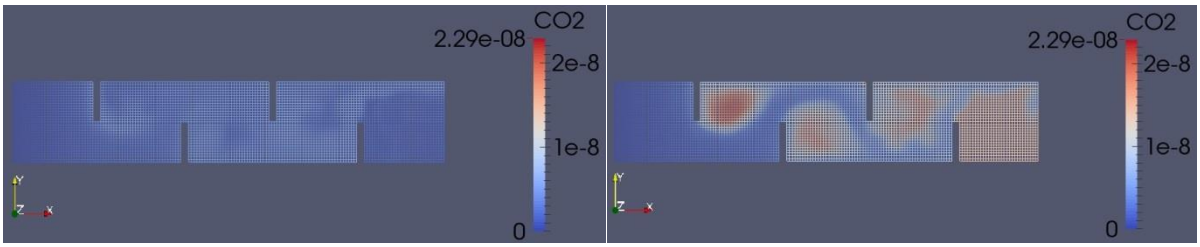

Figure 21: Carbon dioxide distributions in Simulation C

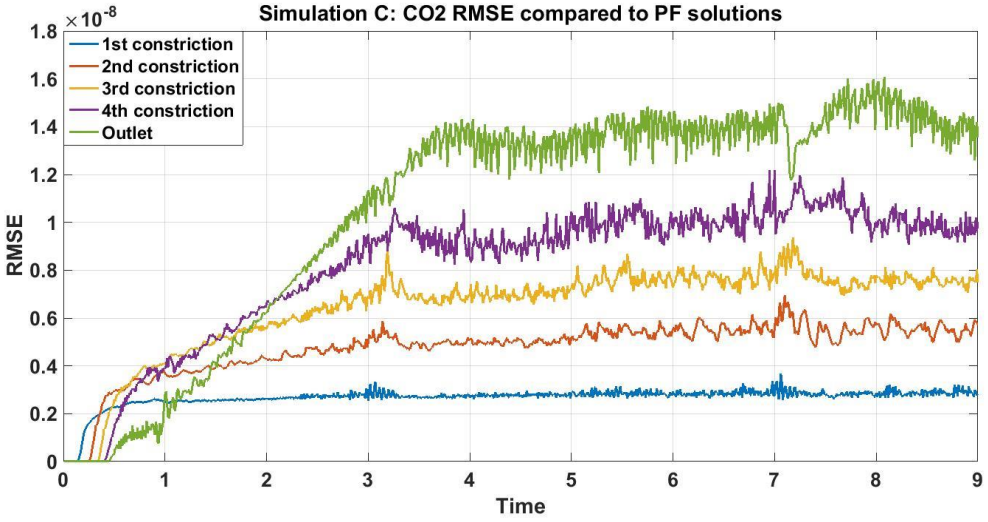

Figure 22: RMSE of carbon dioxide concentration compared to PF solutions

The behaviour of the RMSE values of carbon dioxide concentration with respect to the PF solution (Figure 22) is completely different from that of the RMSE values of biomass concentration. The steady-state value of the RMSE is higher for constrictions that are further away from the inlet, and the RMSE reaches this value more slowly for constrictions that are further away than those that are nearer. This implies that the inaccuracy of the PF solution increases with distance from the inlet, for substances that are produced in reactions within the flow domain. It should be noted that this observation cannot be due solely to the fact that the volume available for accumulation increases with distance, because in calculating the theoretical PF solution the accumulation of carbon dioxide due to reaction was also taken into account.

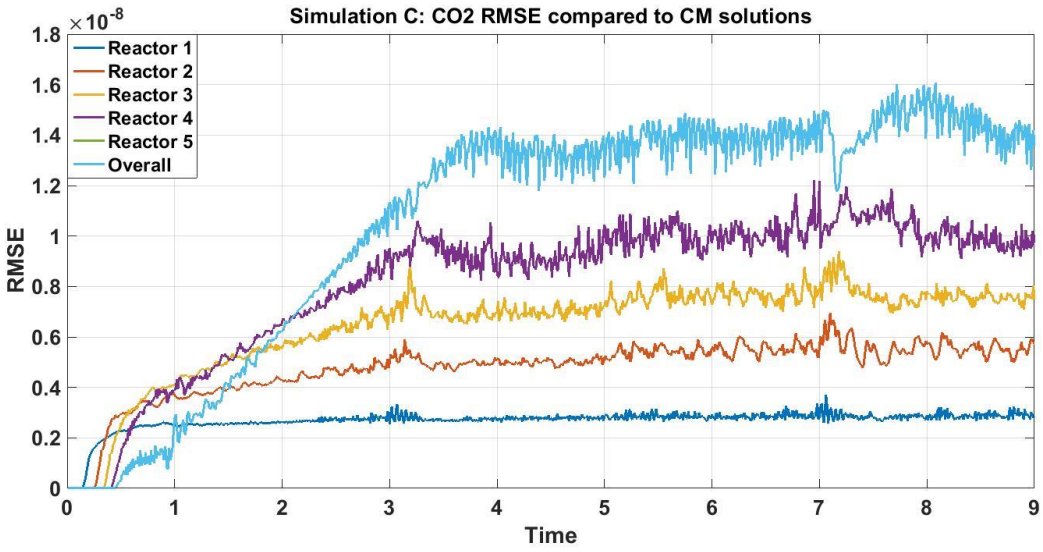

Figure 23: RMSE of carbon dioxide concentration compared to CM solutions

The behaviour of the carbon dioxide RMSE values with respect to the CM solution (Figure 23) is similar to that with respect to the PF solution. Both plots suggest that neither the PF nor CM solution is at all appropriate for modelling the time-dependent concentration profile of substances accumulating due to reaction(s). This is especially so at large distances from the inlet and at steady-state, because the actual solution has converged to that which is significantly different from CM and PF solutions. It should also be noted that the RMSE profile of carbon dioxide concentration in this Simulation C is very different to that of the settling phase in Simulation A. Density effects were not considered in both simulations. Whereas in Simulation A the RMSE of the settling phase was greatest nearest to the inlet, in cases of biological reactions (i.e. this simulation) the RMSE is greatest furthest from the inlet. These observations suggest that the applicability of standard PF and CM models either before or after steady-state is reached is strongly affected by the presence or absence of reactions.

4.4 Comparing the results from simulation D with the analytical solutions for plug flow and complete mixing

A screenshot of the biomass distribution is shown in the Figure 24 below. The 4 well-mixed regions behind the baffles in the direction of flow are again observable, as is the PF flow in-between. The turbulence at the outlet (right) is notable and could be a cause of the RMSE

oscillations at the outlet (see below). Oscillations of the RMSE at the constrictions could also be due to turbulence which induces vortex shedding behaviour at the "interface" between the well-mixed regions and the PF flow.

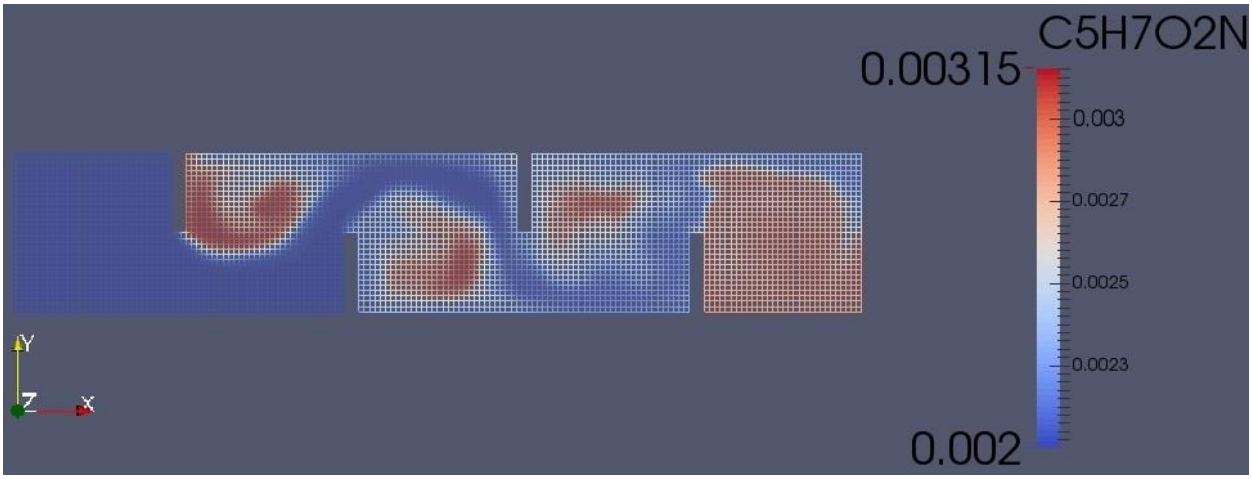

Figure 24: Biomass distribution in Simulation D

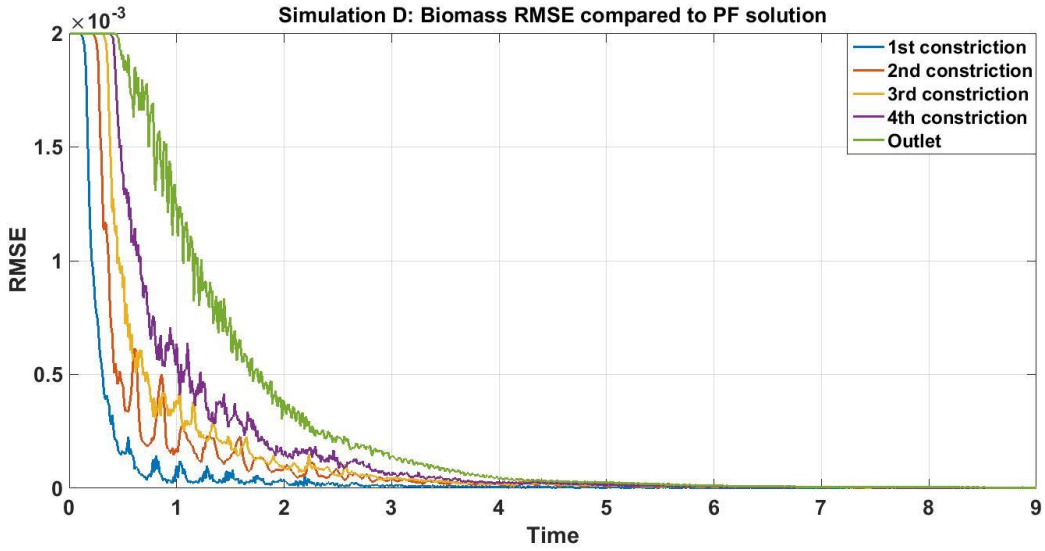

Figure 25: RMSE of biomass concentration compared to the PF solutions

The behaviour of the biomass concentration RMSE with respect to both the PF and CM solutions in Simulation D (Figures 25 and 26) is similar to that in Simulation C. Therefore the inclusion of density effects does not appear to make any significant difference to the time-dependent concentration profiles of reactants. However this could be due more to the fact that gaseous products (carbon dioxide and hydrogen gas) are either dissolved into the fluid mixture

or escape as effervescence, while the remaining liquid and solid components do not have large differences in densities.

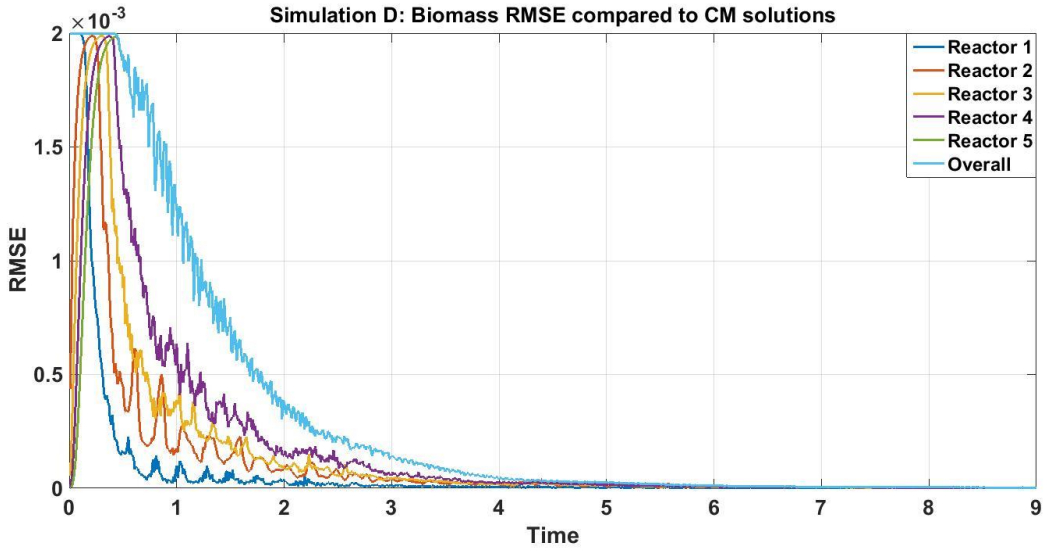

Figure 26: RMSE of biomass concentration compared to the CM solutions

Screenshots of the carbon dioxide distribution are shown in the Figure 27 below (the left at $t = 1.1$ and the right at $t = 3.5$):

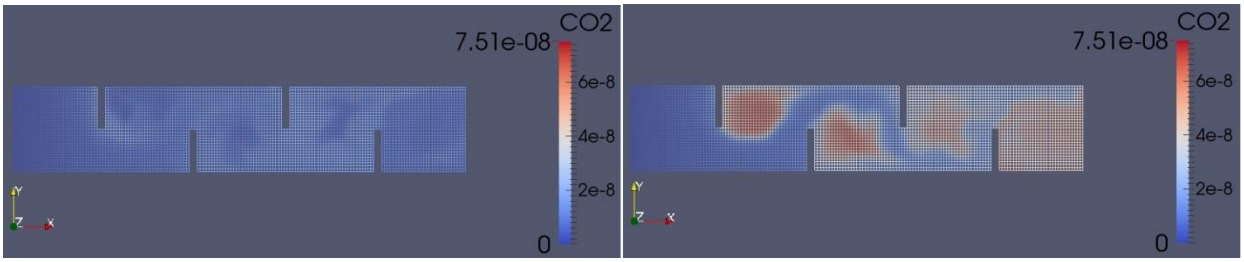

Figure 27: Carbon dioxide distributions in Simulation D

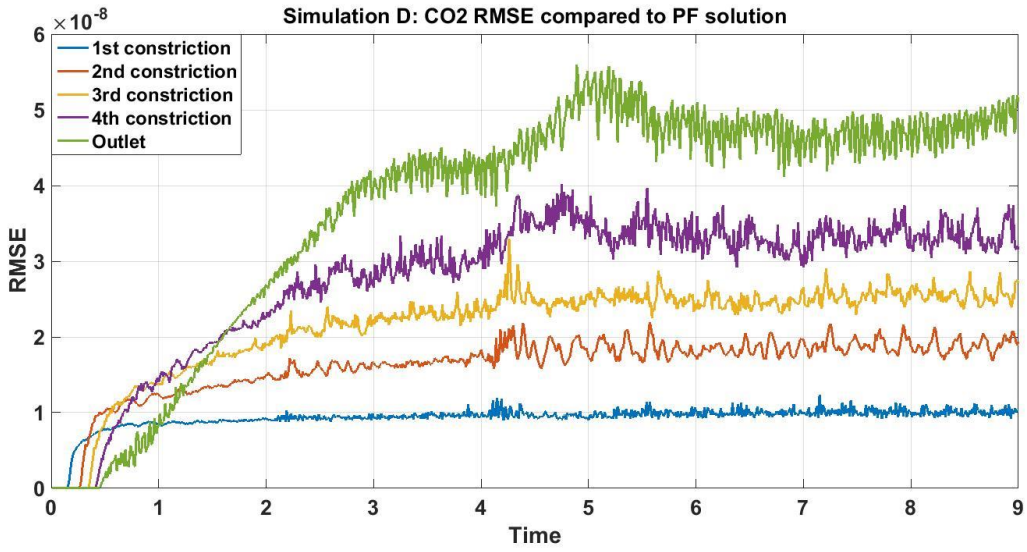

Figure 28: RMSE of carbon dioxide concentration compared to the PF solutions

The behaviours of the RMSE values of carbon dioxide concentration with respect to the PF and CM solutions in this Simulation D (Figures 28 and 29) are similar to that in Simulation C. However, the magnitude of the RMSE values in Simulation D is about 3 times that of those in Simulation C, despite identical reactions and initial conditions. This suggests that the presence of density effects significantly increase the accumulation of reaction products, which is not accounted for by PF and CM models even including reactions.

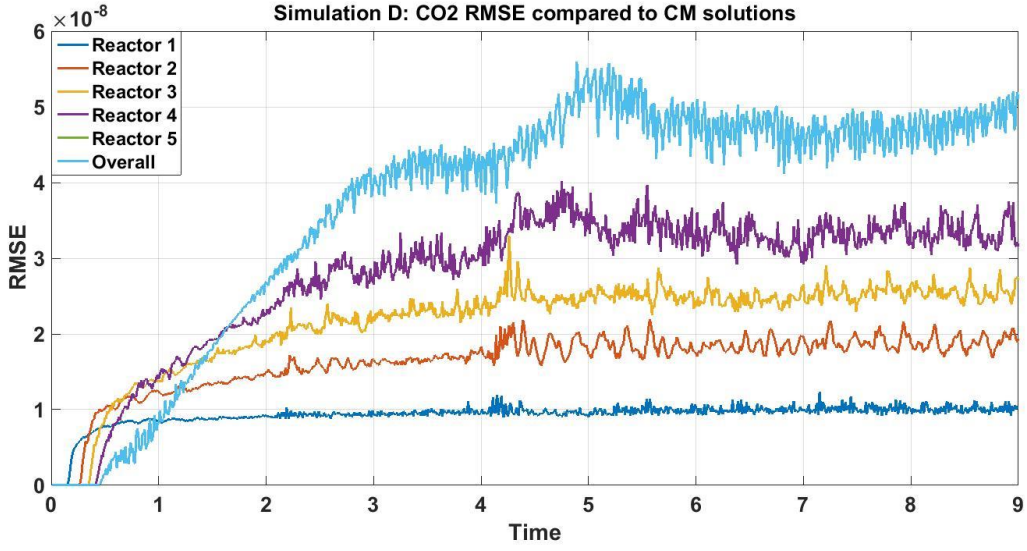

Figure 29: RMSE of carbon dioxide concentration compared to the CM solutions

Simulation D can be used to provide preliminary estimates on the length of time needed to process a given amount of substrate and to achieve a certain of level of bacterial biomass growth. These estimates can be in turn translated into design and operation considerations of reactors and clarifiers which account for both biological and hydrodynamic properties of the processes.

5.0 Conclusions

A protocol for simulating the combined effects of biological reactions and hydrodynamic flow regimes in wastewater treatment processes has been developed. This protocol has been applied to the specific problem of treating high-salinity wastewaters, and has been implemented in the open-source CFD package FreeFOAM. The usage of a novel strain of halophilic bacteria in treating high-salinity waters was considered, and the kinetics of its growth was modelled. The growth model parameters were then used to calculate an appropriate reaction rate constant to be taken as input by FreeFOAM during simulations. An autocatalytic chemical equation was used to represent the overall process of bacterial growth, and FreeFOAM used the reaction rate constant calculated previously to simulate this reaction. The simulations revealed non-intuitive coupled effects between biological reactions and hydrodynamic flow regimes which deviate significantly from the predictions of standard PF and CM models that are commonly used, even after having accounted for reaction terms. The flow properties were such that biological kinetics was not uniform throughout the entire flow domain. This shows that the activated sludge models proposed by the IWA could be significantly enhanced through the inclusion of explicit hydrodynamic modelling. Conversely these results also mean that standard flow models would be augmented by including biological kinetics.

Further work could include re-writing parts of the source code of the chemistry solver used by FreeFOAM. This would enable the concentration of biomass as a function of time to be solved from other models apart from the standard autocatalytic model. Alternatives include the model proposed by Whiting *et al*. (1992), the model of Grau *et al*. (1975), or a combination thereof. For example, the model of Grau *et al*. could be applied to just cells in the log-phase of growth,

or the transition kinetic constants in Whiting's model could be substituted by Monod functions of substrate and inhibitive metabolic waste products. Other areas of further work include applying this protocol to flow domains of different geometries and testing it against a real-world case.

6.0 Risk assessment retrospective

The risk assessment was accurate. No significant hazards were encountered since the work performed as part of the project was deskbound.

7.0 Reduced Bibliography

Burcat, A. (2006). Burcat's Thermodynamic Data. Retrieved May 20, 2015, from http://garfield.chem.elte.hu/Burcat/burcat.html

Droste, R. L. (1997a). Fundamental analysis of plug flow. In C. Robichaud & K. Santor (Eds.), *Theory and Practice of Water and Wastewater Treatment* (1st ed., pp. 258–260). New York: John Wiley & Sons, Inc.

Droste, R. L. (1997b). Mixing Characteristics of Basins. In C. Robichaud & K. Santor (Eds.), *Theory and Practice of Water and Wastewater Treatment* (1st ed., p. 245). New York: John Wiley & Sons, Inc.

Genigeorgis, C., Martin, S., Franti, C. E., & Riemann, H. (1971). Initiation of Staphylococcal Growth in Laboratory Media. *Appl. Envir. Microbiol.*, *21*(5), 934–939. Retrieved from http://aem.asm.org/cgi/content/long/21/5/934

Grau, P., Dohányos, M., & Chudoba, J. (1975). Kinetics of multicomponent substrate removal by activated sludge. *Water Research*, *9*(7), 637–642. doi:10.1016/0043-1354(75)90169-4

Henze, M., Gujer, W., Mino, T., & van Loosdrecht, M. C. M. (2000). Activated Sludge Models ASM1, ASM2, ASM2d and ASM3, 121. Retrieved from http://books.google.com/books?id=W0NTq3LUfOUC&pgis=1

Mathworks. (2014a). Confidence intervals for fit coefficients of cfit or sfit object - MATLAB confint - MathWorks United Kingdom. Retrieved from http://uk.mathworks.com/help/curvefit/confint.html

Mathworks. (2014b). Least-Squares Fitting - MATLAB & Simulink - MathWorks United Kingdom. Retrieved from http://uk.mathworks.com/help/curvefit/least-squares-fitting.html#bq_5kr9-9

Mcbride, B. J., Gordon, S., & Reno, M. A. (1993). Coefficients Thermodynamic Properties for Calculating and Transport of Individual Species. *Nasa Technical Memorandum*, *4513*(NASA-TM-4513), 98. Retrieved from http://ntrs.nasa.gov/archive/nasa/casi.ntrs.nasa.gov/19940013151_1994013151.pdf

Panikov, N. (2002). *KINETICS , MICROBIAL GROWTH*. John Wiley & Sons, Inc. doi:10.1002/0471250589.ebt124

Peterson, M. E., Daniel, R. M., Danson, M. J., & Eisenthal, R. (2007). The dependence of enzyme activity on temperature: determination and validation of parameters. *The Biochemical Journal*, *402*(2), 331–337. doi:10.1042/BJ20061143

Ratkowsky, D. A., Lowry, R. K., McMeekin, T. A., Stokes, A. N., & Chandler, R. E. (1983). Model for bacterial culture growth rate throughout the entire biokinetic temperature range. *J. Bacteriol.*, *154*(3), 1222–1226. Retrieved from http://jb.asm.org/cgi/content/long/154/3/1222

Ratkowsky, D. A., Olley, J., McMeekin, T. A., & Ball, A. (1982). Relationship between temperature and growth rate of bacterial cultures. *J. Bacteriol.*, *149*(1), 1–5. Retrieved from http://jb.asm.org/cgi/content/long/149/1/1

Rittmann, B. E., & McCarty, P. L. (2001). Stoichiometry and bacterial energetics. In *Environmental biotechnology: principles and applications* (p. 754). McGraw-Hill.

Ross, T., & McMeekin, T. A. (1994). Predictive microbiology. *International Journal of Food Microbiology*, *23*(3-4), 241–264. doi:10.1016/0168-1605(94)90155-4

Rosso, L., Lobry, J., Bajard, S., & Flandrois, J. (1995). Convenient Model To Describe the Combined Effects of Temperature and pH on Microbial Growth. *Appl. Envir. Microbiol.*, *61*(2), 610–616. Retrieved from http://aem.asm.org/cgi/content/long/61/2/610

Samaras, C. (2015). Calculating Thermochemical Properties Using The 7 Term NASA Polynomials. Retrieved May 20, 2015, from http://www.myengineeringworld.net/2013/10/Excel-thermochemical-NASA-polynomials-Burcat.html

Tchobanoglous, G., & Burton, F. L. (1991). Nonideal plug-flow reactor. In R. Eliasen, P. H. King, & R. K. Linsley (Eds.), *Wastewater Engineering Treatment, Disposal, and Reuse* (3rd ed., pp. 1265–1273). Irwin/McGraw-Hill.

Zwietering, M. H., Jongenburger, I., Rombouts, F. M., & VAN 'T Riet, K. (1990). Modeling of the Bacterial Growth Curve. *Appl. Envir. Microbiol.*, *56*(6), 1875–1881. Retrieved from http://aem.asm.org/cgi/content/long/56/6/1875